ChemPubSoc Europe

DOI: 10.1002/batt.201900082

BATTERIES & SUPERCAPS
Reviews

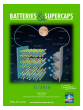

Battery-Type Electrode Materials for Sodium-Ion Capacitors

Xiaoyu Zhao,*[a] Yingbing Zhang,[a] Yanfei Wang,[a] and Huige Wei[a]

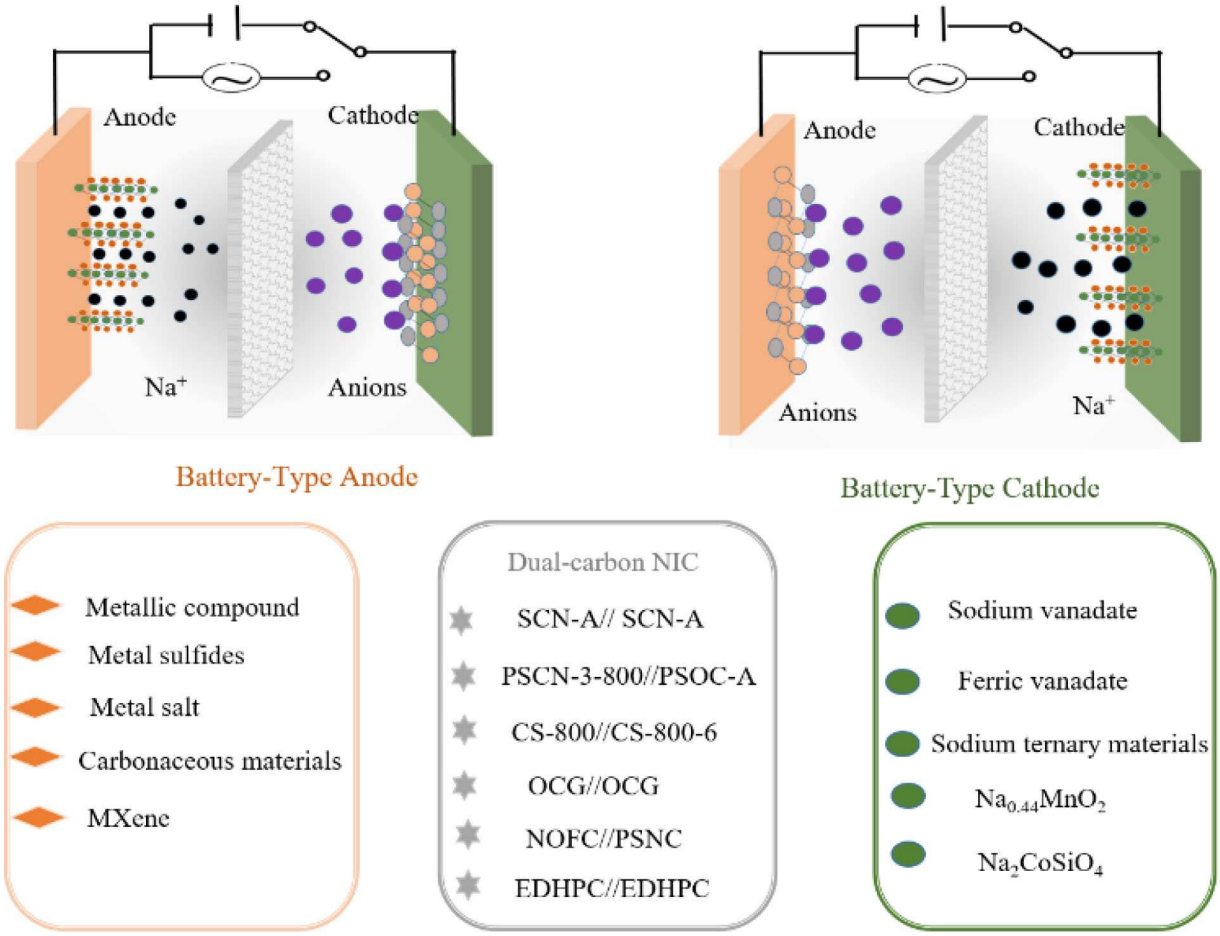

Sodium-ion capacitors (NICs), as a new type of hybrid energy storage devices, couples a high capacity bulk intercalation based battery-style negative (or positive) electrode and a high rate surface adsorption based capacitor-style positive (or negative) electrode, delivering high energy density, high power density, and long lifespan. Since the first NICs have been proposed in year 2012, numerous efforts have been put into searching for appropriate electrode materials to compose NICs devices with improved performance. Especially, battery-type electrode materials carry greater responsibility on performance improvement of NICs. This review provides an overview of electrode materials for NICs according to energy storage mechanisms with an emphasis on battery-type electrode materials design and improved NICs performance. Further, future challenges and perspectives of NICs are also discussed.

1. Introduction

Energy is the important base for economic growth and technology revolution. However, energy consumption/production that relies on the combustion of fossil fuels is forecasted to have a severe future impact on world ecology, such as global warming, melting ice caps, and severe pollution. Renewable energy such as solar, wave, and wind power requires efficient energy storage systems. Electrochemical energy storage is one of the most promising alternative energy storage and release systems.[1] Among various electrochemical energy storage devices, secondary batteries and supercapacitors have drawn wide attention due to their particular advantages.[2] The high energy density for secondary batteries and high power density for supercapacitors make them practical and promising in the energy storage field.[3]

Among diverse secondary batteries, lithium ion batteries (LIBs) were firstly commercialized by Sony in 1991 and investigated intensively. As a result, LIBs are widely applied for electronic devices such as mobile phones, laptops and electrical vehicles today.[4] However, due to the relatively low content and irregular distribution in earth crust and high cost of lithium, the large-scale application and further development of LIBs are restricted to large content. Based on the wide availability and low cost of sodium, sodium-ion batteries (NIBs) are considered as a substitute for LIBs for grid-scale energy storages. Research in the last several years has shown that NIBs are deficient in performance, such as low coulombic efficiency for the first cycle, low power density and relatively short lifetime, which cannot meet the needs for large power devices.[5]

Supercapacitors, enabling the ultra-fast charge and discharge, show extremely high power density and long cycle life but low energy density, compared with lithium ion batteries.[6] The Hybrid ion capacitors are a relatively new type of device that lies between batteries and supercapacitors in terms of energy and power density.[7] Hybrids are attracting increasing scientific attention because of the potential to bridge the energy gap between the two systems. The hybrid ion capacitors couples a high capacity based battery-style negative (or positive) electrode with bulk ions insertion/extraction and a high rate performance based capacitor-style positive (or negative) electrode with surface adsorption/desorption.[8]

In 2001, the first hybrid ion capacitor consisting of nanostructured $Li_4Ti_5O_{12}$ for negative and activated carbon for positive demonstrated an extraordinary energy density of 20 $Wh\,kg^{-1}$ that was three times higher than traditional supercapacitors.[9] After that, various materials, such as graphite, silicon, hard carbon and metal oxides, were applied for lithium ion capacitors (LICs). Similar to LICs, sodium-ion capacitors (NICs) have also drawn researchers' intention widely.

In 2012, the first NICs consisting of porous carbon as positive and sodium titanate nanotubes as negative exhibited high energy and power densities (34 $Wh\,kg^{-1}$ and 889 $W\,kg^{-1}$).[10] In recent years, extensive investigations have been focused on NICs.[11] However, due to the larger ion radius of sodium (0.102 nm) than lithium ions (0.076 nm), most materials applied for LICs cannot be used to NICs without adjusting. The intercalation and deintercalation of sodium ions in materials such as graphite would result in the dramatic change in volume and collapse of structure, which leads to decline of cycling stability of NICs considerably. Therefore, the design and selection of appropriate electrode materials would be of great concern for NICs.[12] Materials with rationally designed structure and morphology are used for sodium-ion storage in half-cells and show excellent electrochemical performance. These materials can also be further used in NICs system. For example, Cu_9S_5@NC,[13] ppy@Sb_2Se_3,[14] SnS@carbon nanotubes,[15] $Fe_{1-x}S$ @PCNWs/rGO,[16] etc.

Regarding the device structure, NICs are similar to NIBs, consisting of positive (cathode), negative (anode), separator and electrolyte. However, different from NIBs that both electrodes store and release energy through reversible faradic reaction, one of electrodes relate to faradic reaction (called battery-type electrode) while the other based on electric double layer (called capacitor-type electrode) involved in fast reversible adsorption and desorption of electrolyte ions on electrode/electrolyte interface for NICs. Thus, NICs are allowed to charge and discharge with higher power density than NIBs, showing excellent rate performance.

Based on the mechanism of energy storage, electrode materials could be classified as capacitor-type and battery-type materials. Various carbon materials with high specific surface areas and high electrical conductivity are the typical capacitor-type materials, storing energies by absorbing electrolyte ions on the surface of electrode to forming electrical double layer structure.[17] Modification strategy of these materials has been

[a] Dr. X. Zhao, Y. Zhang, Prof. Y. Wang, Dr. H. Wei
Tianjin Key Laboratory of Brine Chemical Engineering and Resource Eco-utilization, College of Chemical Engineering and Materials Science, Tianjin University of Science and Technology, Tianjin 300457, China
E-mail: xyz@tust.edu.cn

focused on the improvement of specific area surface and optimization of porous structure.[18] Battery-type materials, including metallic compound, metal salt, and hard carbon, store energies by Faradic reactions occurring in the bulk of electrode materials. The insertion/extraction occurs not only in the near surface but also in the bulk of the material. The Na^+ storage capacities of battery-type materials could be improved largely owning to its more extensive modification strategies. Herein, modification strategies and corresponding improvements of battery-type materials for NICs are summarized and discussed.

2. Energy Storage Mechanism and Classification

According to the different electrode materials, the energy storage mechanism could be classified as electrical double layer and faraday redox reaction. For the former mechanism, electrolyte ions are adsorbed on the interface between electrode and electrolyte to form electrical double layers (Figure 1). The used electrode materials with high specific area and stability are carbon materials such as activated carbon, graphene and carbon nanotube.[19] The faraday pseudocapacitance indicates that the electroactive substance is subjected to under potential deposition in a two-dimensional space on the surface or in the bulk phase, with rapid reversible redox reactions to store the charge. In the process of energy storage and conversion, sodium ions in the organic electrolyte intercalate and deintercalate the electrode material, while the electrical energy and chemical energy converse mutually. During charging sodium ions deintercalates from the lattice of the positive material and migrate through the membrane and the electrolyte to the negative under the driving of the external potential. Meanwhile electrons migrate from positive to negative through the external circuit and are captured by sodium ions to form sodium metal. The electrical energy from the external circuit is converted into chemical energy and stored in the negative electrode material. During discharging the metal sodium stored in the negative electrode convert into sodium ions which migrate through the electrolyte and the membrane to the positive electrode and intercalate in the crystal lattice of the positive electrode material. In the ideal condition, the intercalation and deintercalation of sodium ions only cause a change in the interlayer spacing of the electrode without collapse of the crystal structure.[20]

3. Battery-Type Anode Materials

Normally carbon materials with high specific area and abundance pores, such as activated carbon, are employed for capacitive electrode. Meanwhile, diverse metallic compound, metal salt, carbonaceous materials and MXene capable to reaction with Na^+ have been applied for battery electrode. In this chapter, these materials are summarized and discussed in detail.

3.1. Metallic Compound

3.1.1. Titanium Dioxide

Various polymorphs of titanium dioxide (TiO_2), including amorphous TiO_2 nanotubes, TiO_2 (B), rutile, and undoped anatase TiO_2, have received a great deal of attention, to sodium ions storage. Among these polymorphs, TiO_2 is intensively used as anode electrode material in NICs due to its abundant reserves, stable structure, low price, and environment-friendly. Anatase-type TiO_2 could deliver a high theoretical capacity of 335 $mA\,h\,g^{-1}$ with a low insertion potential of 0.7 V.[21] However, as a semiconducting material, its electronic conductivity is poor inherently. In order to improve its electronic conductivity,

Xiaoyu Zhao is currently an associate professor in the College of Chemical Engineering and Materials Science in Tianjin University of Science and Technology. He obtained his Ph. D. degree from University of Fukui in 2014. His research fields include interface electrochemical theory and its application in energy storage and separation & sensing technology.

Yingbing Zhang is pursuing his M.S. in the College of Chemical Engineering and Materials Science in Tianjin University of Science and Technology. Her research interests focus on sodium-ion capacitors.

Yanfei Wang is currently a professor in the College of Chemical Engineering and Materials Science in Tianjin University of Science and Technology. He obtained his Ph.D. degree from Tianjin University in 2005. His research interests include comprehensive utilization of marine and brine resources and engineering technology.

Huige Wei is currently an associate professor at College of Chemical Engineering and Materials Science in Tianjin University of Science and Technology. She obtained B.S. and M.E. degree from Harbin Institute of Technology in 2009 and 2011. She obtained his Ph.D. degree from Lamar University in 2015. Her research interests include multifunctional nanocomposites in energy conservation, energy storage and corrosion resistance of metal.

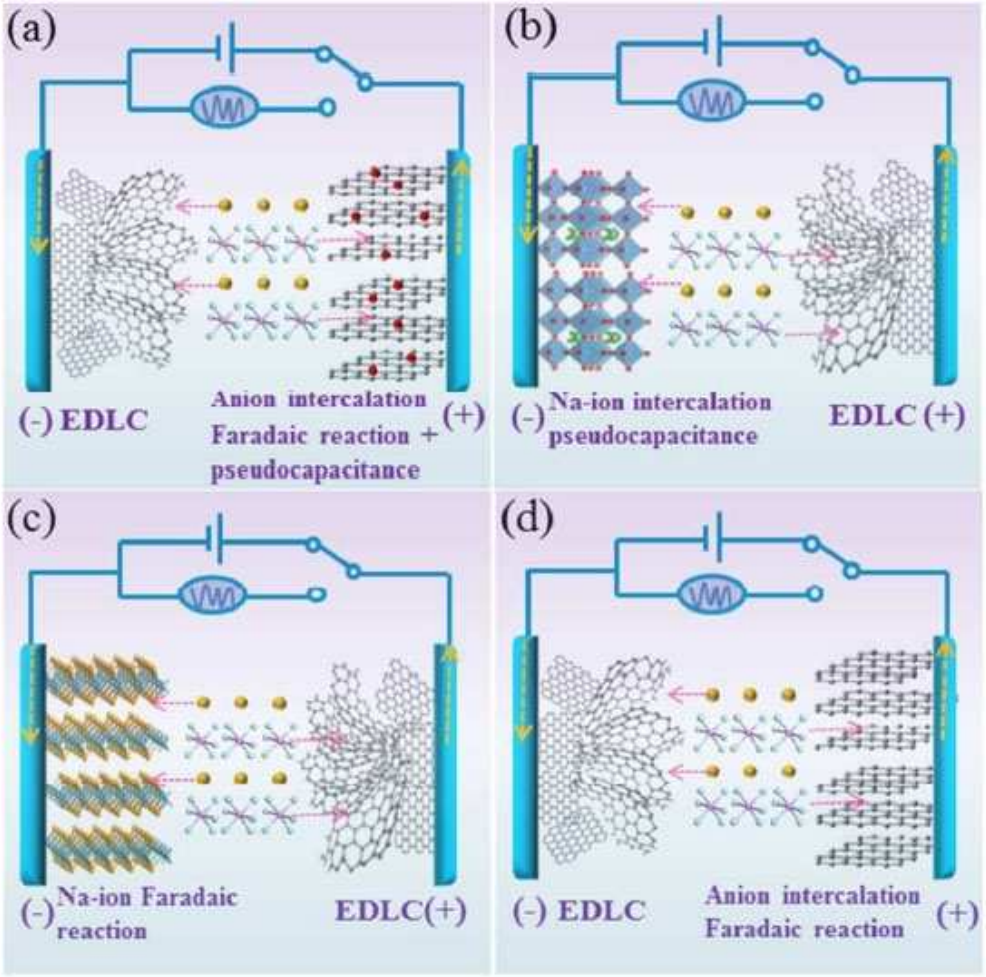

Figure 1. Schematic illustration of working principles of (a) this Na-ion hybrid capacitor and (b–d) conventional Na-ion hybrid capacitors. Dotted lines in red and yellow mean the transfer of ion and electron, respectively. Redrawn from Ref. [13b].

various method have been investigated to design innovative TiO_2 to achieve improved electrochemical performance, such as reducing the particle size,[22] coating with graphene,[23] heteroatom doping,[24] and morphology control.[25]

Passerini and co-workers[26] utilized in situ XRD and ex situ XPS to study the energy storage mechanism of TiO_2. During the first cycle discharge, the XRD lattice of anatase TiO_2 has a slight shift at low angle, which indicates that the lattice of anatase continues to expand. However, when the discharge potential is less than 0.3 v, the XRD peak of anatase disappears, and the peak still does not appear after charging, which indicates that the TiO_2 structure is rearranged. In the process of circulation, it becomes amorphous structure. Ex situ XPS, SEM and Raman analysis showed that sodium embedded in TiO_2 reduced Ti^{4+} to Ti^{3+} and partially formed Ti and NaO_2.

Electrical conductivity of TiO_2 can be enhanced effectively and efficiently by Nitrogen doping and introduction of oxygen vacancies, which conduces to its electrochemical performance. Liu and co-workers[24a] synthesized nitrogen doping anatase TiO_2 tiny nanospheres (N-TiO_2) that exhibited a stable capacity of 162 mA h g^{-1} over 1000 cycles at 1 A g^{-1} and superior rate performance in a half-cell. When assembled a NICs with an N-TiO_2 anode and an activated carbon cathode, the N-TiO_2//AC device delivered high energy and power densities (80.3 Wh kg^{-1} and12500 W kg^{-1}), as well as excellent long term cycling stability up to 6500 cycles. In addition, molybdenum and niobium doping can also greatly improve the electrochemical performance of TiO_2. Bauer and co-workers[24b] prepared Mo-doped titania ($Mo_{0.1}Ti_{0.9}O_2$) and Nb-doped titania ($Nb_{0.25}Ti_{0.75}O_2$) and applied for NICs. As shown in Figure 2a–f, TEM images revealed that particle morphology and size did not differ significantly between undoped and doped TiO_2 samples. The synthesized materials performed significantly better than the undoped counterpart (Figure 2g, 2h), largely taking advantage of the pseudocapacitive charge storage and improved sodium-ion diffusion. The resulting $Mo_{0.1}Ti_{0.9}O_2$//AC NIC showed the highest energy densities of 60 Wh kg^{-1} at a power density of 350 W kg^{-1}, and delivered a wide voltage window of 1–3 V with 75% capacity retention after 3000 cycles. Other reported works with TiO_2-based materials as anode in NICs are summarized in table 1. The TiO_2-based NICs usually exhibit outstanding power density and long cycle life due to the pseudocapacitive reaction with Na ions, but their energy densities need to be further improved.

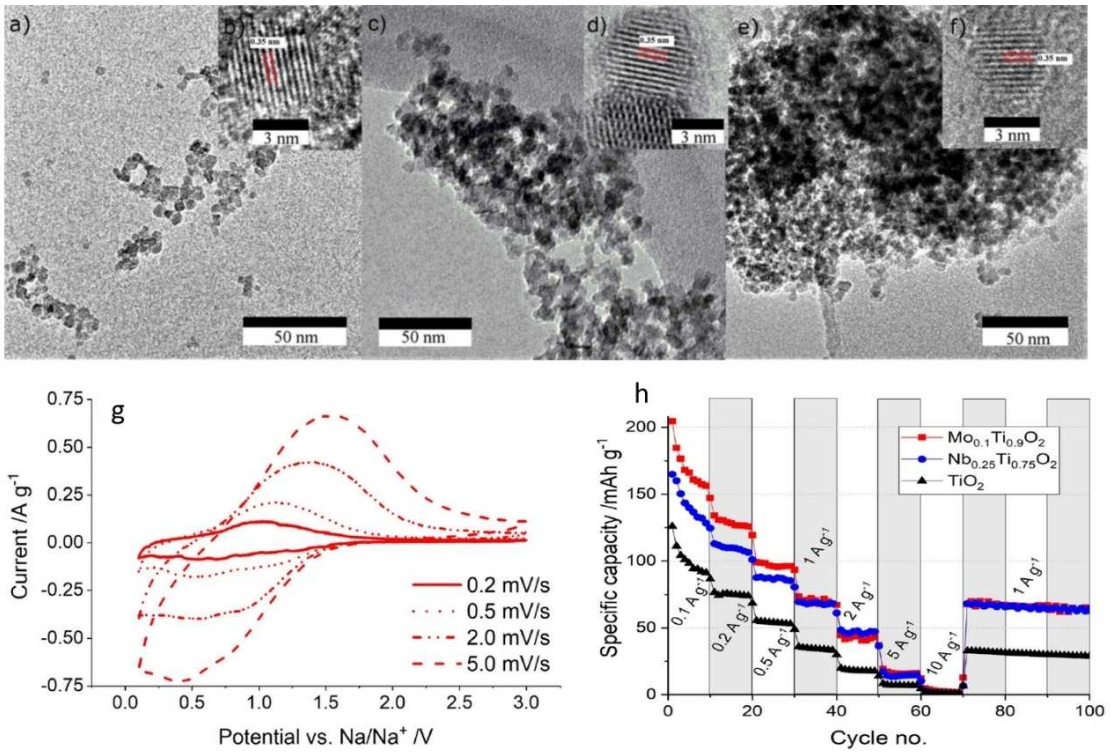

Figure 2. TEM images showing an overview of particles of (a) TiO_2, (c) $Mo_{0.1}Ti_{0.9}O_2$ and (e) $Nb_{0.25}Ti_{0.75}O_2$, as well as images showing lattice fringes for (b) TiO_2, (d) $Mo_{0.1}Ti_{0.9}O_2$ and (f) $Nb_{0.25}Ti_{0.75}O_2$. (g) Cyclic voltammetry shows the anode and cathode currents of $Mo_{0.1}Ti_{0.9}O_2$ divided by the square root of scan rate. (h) Charge/discharge testing at varying specific currents for tens of cycles in Na-ion half-cells. Redrawn from Ref. 24b.

3.1.2. Nb_2O_5

Niobium pentoxide (Nb_2O_5) is regarded as a promising energy storage material for Na^+ storage due to its high power characteristics and cycling stability.[27] However, the transition metal oxide electrode often has problems such as low reversible capacity and slow redox kinetics, which seriously restrict the rate performance of the device. Li and co-workers[28] demonstrated a hybrid NICs utilizing self-assembled Nb_2O_5 nanosheets as anode and peanut shell derived carbon as the cathode, which delivered energy density of 43.2 Wh kg^{-1}, power density of 5760 W kg^{-1}, and stable cycle life with capacity retention of 80% after 3000 cycles in the wide potential range of 1–3 V. Zhong and co-workers[29] prepared uniform sandwich-like mesoporous Nb_2O_5/graphene/mesoporous Nb_2O_5 (G@mNb_2O_5) nanosheets and used as anode for NIC. The mesoporous Nb_2O_5 layers were assembled by nanometer-sized Nb_2O_5 particles, as shown in Figure 3a–d. Taking advantage of the rational structural design, the charge and discharge curves of the prepared G@mNb_2O_5 nanosheets electrode demonstrated similar profile at various current densities from 50 to 4000 mA g^{-1}, as shown in Figure 3e–f. Benefit from improved surface pseudocapacitance, the rapid redox kinetics, the short characteristic relaxation process and increased sodium-ion diffusion coefficient, the as-assembled G@mNb_2O_5//AC NIC device demonstrated an excellent energy density (56.1 Wh kg^{-1} and 9.7 Wh kg^{-1} at 120 W kg^{-1} and 7200 W kg^{-1}, respectively) and remarkable cycling stability as shown in Figure 3g.

3.1.3. Metal Sulfides

Metal sulfides, with various crystal structures, valence states and nanocrystalline morphologies have been widely applied for energy storage devices, such as LIBs, NIBs and supercapacitors. Compared with corresponding metal oxides, metal sulfides usually have better electrical conductivity, mechanical properties, thermal stability and rich redox chemistry, which allow them to be practical and promising candidate of anode materials for NICs as well. Metal sulfides applied for NICs include non-layered sulfides (FeS, FeS_2 Sb_2S_3) and layered disulfides (SnS_2, MoS_2).

As a typical non-layered sulfide, ferrous sulfide (FeS_2) has advantages of abundant resources, low price and high theoretical specific capacity when used to sodium ions storage. Due to multiple redox reactions upon cycling, the voltage plateaus of FeS_2 overlap severely, which restricts their application for sodium-ion batteries but favors their usage to NICs. Long and coworkers[30] prepared solid solution of S/Se in $FeS_{2-x}Se_x$ (Figure 4a–b), on the basis of the structure demonstrated in Figure 4d, combining the high specific capacity of FeS_2 and the good redox kinetics of $FeSe_2$ (Figure 4e–f). The resulted material exhibited excellent cycle stability (220 mA h g^{-1} after 6000 cycles at 2 A g^{-1}) and superior rate capability (210 mA h g^{-1} at 40 A g^{-1}) within 0.8–3.0 V. As shown in Figure 4c, In the charge process, Na^+ intercalated into $FeS_{2-x}Se_x$, and meanwhile ClO_4^- in the electrolyte migrate and adsorb to the cathode surface. During the discharge process, Na^+ is

Table 1. Performance of NICs composed of battery-type anode.

Anode//Cathode	electrolyte	Potential range [V]	Max energy density [Wh kg^{-1}]	Max power density [W kg^{-1}]	Cycling life	Year	Ref.
N-TiO_2//AC	1 M $NaPF_6$ (EC/DMC/EMC)	1–4	80.3	12500	6.5 K cycles	2016	[24a]
$M_{00.1}Ti_{0.9}O_2$//AC	1 M $NaPF_6$ (EC/DEC)	1–3	60	10650	75%@5 mA/cm^2 after 3k cycles	2018	[24b]
TiO_2 nanotubes//AC	1 M $NaPF_6$(PC)	1–4	68	12500	80%@1 A/g after 10k cycles	2018	[25a]
TiO_2@CNT@C//bioderived active carbon	1 M $NaClO_4$ (EC/PC)	1–4	81.2	12400	85.3%@1 A/g after 5k cycles	2017	[40]
Graphene TiO_2//Carbon-based	1 M $NaClO_4$ (EC/PC/FEC)	1–4	64.2	1357	90%@10 C after 10k cycles	2017	[23]
TiO_2/CFC//CFs	1 M $NaPF_6$ (EC/DMC/EMC)	1.2–4.3	73.8	13750	90%@1 A/g after 4k cycles	2017	[22]
M-TiO_2-rGO//PDPC	1 M $NaClO_4$ (EC/DEC/FEC)	1–4	94.7	4093	64%@2 A/g after 2k cycles	2018	[41]
TiO_2/C//ZDPC	1 M $NaClO_4$ (EC/PC/FEC)	1–4	142.7	25000	90%@1 A/g after 10k cycles	2018	[25b]
TiOxNy/C//NHPC	1 M $NaClO_4$ (EC/DEC/FEC)	0–4	80	2000	90%@0.8 A/g after 1.2k cycles	2018	[42]
Nb_2O_5 nanosheets//PSC	1 M $NaClO_4$ (EC/PC/FEC)	1–3	43.2	5760	80%@1.28 A/g after 3k cycles	2016	[28]
Nb_2O_5@C/rGO//(MSP-20) AC	1 M $NaPF_6$ (EC/DMC/FEC)	1–4.3	76	20800	63%@1 A/g after 3k cycles	2016	[43]
G@mNb_2O_5//AC	1 M $NaClO_4$ (EC/PC/FEC)	0–2.4	56.1	7200	99%@1 A/g after 4.8k cycles	2018	[29]
Gr- Nb_2O_5//AC	1 M $NaClO_4$ (EC/DMC/FEC)	0–3	112.9	5330	97.1%@1 A/g after 1.5k cycles	2018	[44]
m-Nb_2O_5/CNF//GF/mCNF	1 M $NaClO_4$ (PC/FEC)	0–4	124	60000	80%@2 A/g after 3k cycles	2019	[45]
$FeS_{2-x}Se_x$//AC	1 M $NaClO_4$	0–3	67	2543	60%@1 A/g after 1k cycles	2018	[30]
3D-IO FeS-QDs@NC// AC	1 M $NaClO_4$ (EC/PC/FEC)	0.5–3.5	151.8	9280	91%@1 A/g after 5k cycles	2019	[46]
MoS_2@BPC//BPC	1 M $NaClO_4$ (PC/FEC)	0–4	112.2	8333	90%@2 A/g after 1k cycles	2018	[47]
MoS_2/G//MoS_2/G	1 M $NaClO_4$ (EC/PC/FEC)	0.1–2.5			50 F/g@1.5 C after 2k cycles	2014	[48]
MoS_2/rGO//MoS_2/rGO	1 M $NaPF_6$ (EC/DEC)	0–3	52	60	77%@0.13 A/g after 2k cycles	2019	[49]
MoS_2/C@CC//AC@CC	1 M $NaClO_4$ (EC/DMC/FEC)	0–4			83.3%@ 1 mA/cm^2 after 0.2k cycles	2018	[33]
N/S-HCNFs//AC	1 M $NaClO_4$ (EC/DMC/FEC)	0–4	116.4	20000	81%@2 A/g after 3.5k cycles	2019	[50]
MnO_2@rGO//CGH	0.75 M $NaPF_6$ (EC/DEC)	0–3	79	95	78%@0.07 A/g after 1k cycles	2018	[37]
$MoSe_2$/graphene//AC	1 M $NaClO_4$ (EC/DEC/FEC)	0.5–3	82	10752	81%@5 A/g after 5k cycles	2018	[51]
O-$MoSe_2$/SnO_2//AC	1 M $NaClO_4$ (EC/DEC/FEC)	0.5–3	70	2304	94%@5 A/g after 6k cycles	2018	[52]
$MoSe_2$/MnO_2-graphene//AC	1 M $NaClO_4$ (EC/DEC/FEC)	1–3.4	71	14316	92%@6 A/g after 7k cycles	2018	[53]
$NbSe_2$//AC	1 M $NaClO_4$ (EC/PC/FEC)	0–3	41.7	599.6	93.2%@0.3 A/g after 3k cycles	2019	[54]
V_2O_5/rGO//AC	0.75 M $NaPF_6$ (EC/DEC)	0.01–3	65	72	74%@0.06 A/g after 1k cycles	2017	[38]
m-WO_{3-x}@nm-rGO// MSP-20	1 M $NaPF_6$ (EC/DMC/FEC)	1.0–4.3	67	21000	@1 A/g after 1k cycles	2017	[55]
SnS/aCMT//aCMT	1 M $NaClO_4$ (EC/DMC/FEC)	0.5–4	115		83%@1 A/g after5k cycles	2019	[56]
$CoWO_4$/RGO//AC	1 M $NaClO_4$	1–4.2	87.2	1120.7	100%@0.1 A/g after1k cycles	2018	[57]
$Na_2Ti_3O_7$@CNT//PSC	1 M $NaClO_4$ (EC/PC/FEC)	0–3	58.5	3000	75%@0.4 A/g after 4k cycles	2015	[58]
$Na_2Ti_3O_7$//PSC	1 M $NaPF_6$ (EC/DEC)	0.5–3.5	111.2	11200	86%after 3k cycles	2016	[59]
$Na_2Ti_9O_{19}$//AC	1 M $NaPF_6$ (EC/DMC)	1–4.5	54	5000	75%@2 A/g after 2k cycles	2018	[60]
$Na_2TiO_4(OH)_2$//AC	1 M $NaPF_6$ (PC)	1–4	65	18750	93%@1 A/g after 3k cycles	2017	[61]
$NaTi_2(PO_4)_3$//AC	1 M $NaClO_4$ (PC)	0–2.5	56	4096	100%@5 A/g after 20k cycles	2017	[62]
$NaTi_2(PO4)_3$@rGO//AC	1 M $NaClO_4$ (EC/DMC)	0–2.7	53	6080	98%@10 C after 5k cycles	2017	[63]

Table 1. continued

Anode//Cathode	electrolyte	Potential range [V]	Max energy density [Wh kg^{-1}]	Max power density [W kg^{-1}]	Cycling life	Year	Ref.
$NaTi_2(PO_4)_3$@CNs//CNs	1 M $NaClO_4$ (EC/DEC)	0–3	80	8000	90%@4 A/g after 75k cycles	2017	[64]
$Na_3V_2(PO_4)_3$//CMK-50 carbon	1 M $NaClO_4$ (EC/DMC)	0–3	54	2200	5k cycles	2018	[65]
$Na_3V_2(PO_4)_3$@C//CDC	1 M $NaClO_4$ (EC/DEC)	0–3	118	850	95% after 10k cycles	2016	[66]
$Na_3V_2O_2(PO_4)_2F$@PEDOT// AC	1 M $NaClO_4$ (EC/PC/FEC)	1–4.2	158	7000	85.1%@1 A/g after 1k cycles	2019	[67]
$NiCo_2O_4$//AC	1 M $NaClO_4$ (PC/DMC)	0–4.5	23.5	308	61.2%@0.15 A/g after 2k cycles	2013	[68]

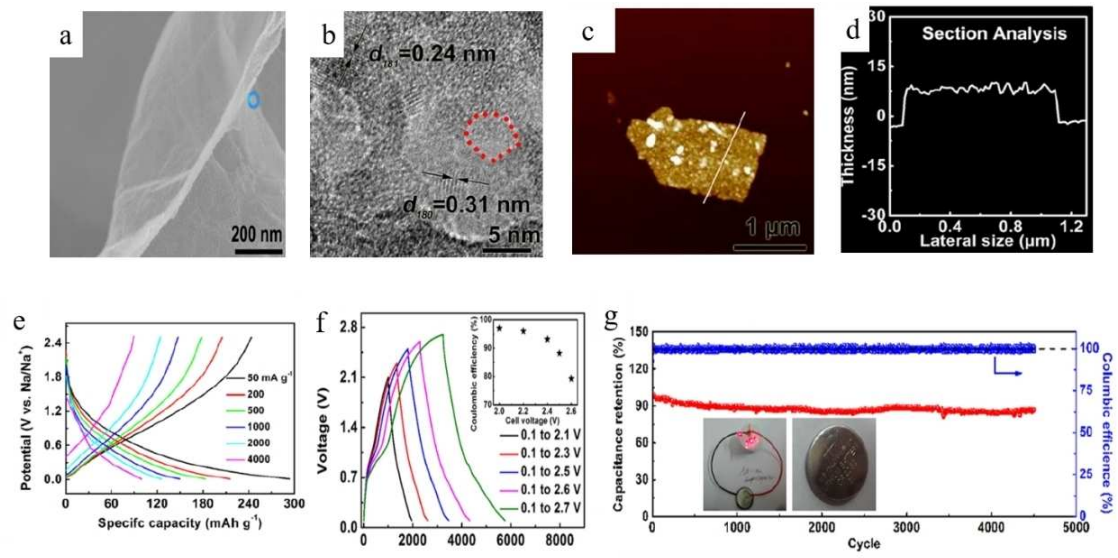

Figure 3. (a) SEM and (b) top-view HRTEM image of the G@mNb_2O_5 nanosheets. (c), (d) AFM image of one G@mNb_2O_5 nanosheet and the corresponding height-profile analysis along the white line. Galvanostatic charge/discharge profiles of (e) G@mNb_2O_5 nanosheets electrode and (f) a G@mNb_2O_5//AC devices. (g) Cycling performance of G@mNb_2O_5//AC device. Redrawn from Ref. [29].

deintercalated from $Na_yFeS_{2-x}Se_x$ and ClO_4^- return to the electrolyte, the fabricated $FeS_{2-x}Se_x$//AC hybrid NICs device delivered a maximum energy density of 67 Wh kg^{-1} and a maximum power density of 2543 W kg^{-1} with 60% capacitive retention after 1000 cycles.

Obviously, rapid capacity decay and poor electrical conductivity are inherent shortcomings of sulfide. Adjusting the structure and improving the conductivity of these anode materials at the nanoscale would be effective strategies to solve these problems. Lou and co-workers[31] proposed a multistep template method to synthesize hierarchical double-shelled nanoboxes with the CoS_2 nanosheet-constructed outer shell supported on the CuS inner shell. Complex nanostructures and chemical compositions thus improved electrochemical performance, high capacity, high rate, long cycle life and possibly possess other advantages. So design and construction of nano structure may leads to another potential direction for researches on NICs electrode materials.

Molybdenum disulfide (MoS_2) is a typical layered disulfide, which shows two-dimension layer structure with a certain interlayer distance of 0.645 nm, providing an efficient slit-like sodium-ion diffusion channel.[32] Chen and co-workers[33] synthesized carbon-coated MoS_2 nanosheets by hydrothermal reaction on carbon cloth (CC) substrates. The unique structure take advantage of extended interlayer distance of MoS_2 ensuring high ion mobility and the highly conductive CC providing a structure support to prevent re-stacking of the MoS_2 sheets during cycling. The prepared anode illustrated a high area capacity of 0.511 mA h cm^{-2} at a current density of 0.2 mA cm^{-2} and 83.3% capacity retention after 200 cycles at 1 mA cm^{-2}. The fabricated NIC of MoS_2/C@CC//AC@CC provided a high energy density of 1.22 mW h cm^{-2} at 0.76 mW cm^{-2}, showing an excellent energy power delivery.

A rationally designed composite of TiO_2-coated MoS_2@N-doped carbon has been applied for anode material of NICs. Due to the ALD TiO_2 coating layer, charge-transfer resistance of TiO_2-coated MoS_2@N-doped carbon is larger than the sample

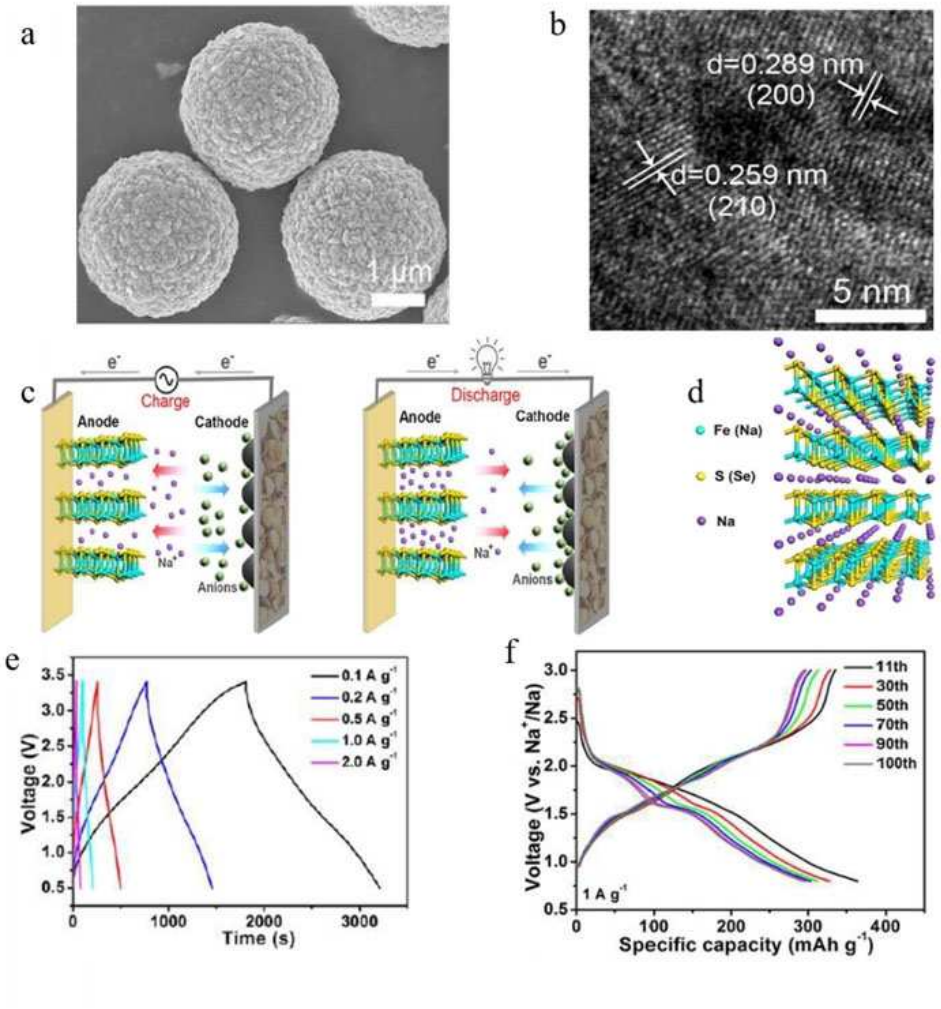

Figure 4. (a) SEM and (b) HRTEM image of $FeS_{1.6}Se_{0.4}$. (c) Schematic diagram of the charge and discharge processes of $FeS_{2-x}Se_x$//AC. (d) Crystal structure of layered-structure $Na_2FeS_{2-x}Se_x$. (e) $FeS_{2-x}Se_x$//AC and (f) $FeS_{1.6}Se_{0.4}$. Reprinted from Ref. [30] with permission from American Chemical Society. Copyright (2018) American Chemical Society.

without coating at early cycles. After 200 cycles the R_{ct} of both products is decreased because of expanded and exfoliated interlayers. However, TiO_2-coated MoS_2@NC exhibited lower R_{ct} due to more stable electrode structure by the TiO_2 protection. Ex-situ XRD of the electrode after 1st and 500th cycle indicated the layered structure of MoS_2 was protected well with TiO_2 layer. In addition, Ex-situ TEM images demonstrated the electrode architecture of TiO_2/MoS_2@NC after 500 cycles could be maintained better than the products without ALD TiO_2 because TiO_2 coating can protect the interface. Based on the unique structure, The TiO_2/MoS_2@NC electrode exhibited a high discharge capacity (351.3 mAh g^{-1} at 20 A g^{-1}), excellent rate performance (~67% capacity retention from 0.1 to 20 A g^{-1}) and superior cycling stability (no capacity decay at 2 A g^{-1} after 500 cycles).[34]

3.1.4. Other Metallic Materials

Other metal compounds, such as MoO_2, V_2O_5, and $MoSe_2$ with advantages of low resistivity, high specific capacitance and environmental friendliness, are used as anodes for NICs.[35] Normally, MoO_2 are combined with carbon materials especially graphene to promote chemical stability, mechanical strength and a viable approach to the electrochemical reaction.[36] Nithya and co-workers[37] synthesized MoO_2@rGO composite materials as an anode and biomass derived activated carbon cathode for NICs. The as-assembled MoO_2@rGO//CGH NIC device showed energy density of 79 Wh kg^{-1} and power density of 95 W kg^{-1} at the current density of 0.04 A g^{-1} with 78% capacity retention after 1000 cycles at 2 A g^{-1}.

Vanadium oxide (V_2O_5) undergoes bulk ion insertion and extraction reaction during reversible charge and discharge, producing a capacitor like sloping profile when employed as an anode for NICs. However, V_2O_5 shows poor electrical conductivity (~10^{-6} S cm^{-1}) and high plateau, which restricts its application for NIC. Graphene coating and nanocrystallization are

efficient methods to solve the problem, which improves not only the electrical conductivity but the ion diffusion kinetics. Kiruthiga and co-worker[38] prepared V_2O_5 nanorods loaded on rGO as anode electrode and honey-derived carbon as cathode. The fabricated V_2O_5/rGO//AC hybrid NICs device exhibited a maximum energy density of 65 Wh kg^{-1} and a maximum power density of 72 W kg^{-1}, with an excellent capacitive retention of 74% even after 1000 cycles at 0.06 A g^{-1}.

Transition metal selenides especially two-dimensional selenides have become the research hotspot of negative electrode materials for sodium-ion batteries in recent years due to their low cost and high theoretical specific capacity. Although compared with the metal oxide conductivity is relatively large, with the high conductivity of carbon-based materials are still a big gap. And the volume effect is obvious in the charging and discharging process. Lou and co-workers[39] using the simulated micro-cube of co-co Prussian blue as the raw material, the $CoSe_2$ micro-box of layered doped copper assembled from ultra-thin nano-sheets was synthesized by two-step ion exchange method. These hierarchical $CoSe_2$ microboxes are doped with Cu^{2+} ions through a subsequent cation-exchange reaction with Cu^{2+} ions. Cu–$CoSe_2$ microboxes has high reversible capacity, good rate capacity and good cyclic stability, which improves the sodium storage performance

More reported works with metallic materials as anode in NICs are summarized in table 1. These metallic materials, such as various TiO_2 composites, Nb_2O_5 composites, FeS_2 composites, MoS_2 composites, $MoSe_2$ composites, MnO_2 composites, $NbSe_2$ composites, V_2O_5 composites, WO_3 composites, SnS composites, $CoWO_4$ composites, $Na_2Ti_3O_7$ composites, $NaTi_2(PO_4)_3$ composites, $Na_3V_2(PO_4)_3$ composites and $NiCo_2O_4$ composites, are potential candidates for anode materials of NICs and need to be investigated further. The corresponding cathodes, electrolyte, potential, max energy density, max power density and cycling life are also listed in the table. The max energy density of listed NICs are below 100 Wh kg^{-1}, and the capacities remains at least 80% after several thousand cycles. Remarkably, $NaTi_2(PO_4)_3$@CNs//CNs, $NaTi_2(PO_4)_3$//AC and TiO_2/C//ZDPC devices show high capacity retention after 75000, 20000 and 10000 cycles, respectively. NASICON type materials show improved electrochemical performance after heteroatom doping and coating with conductive polymer. On the other hand, corresponding cathode, employ mostly activated carbon or biomass derived carbon.

3.2. Metal Salt

3.2.1. $NiCo_2O_4$

$NiCo_2O_4$ is usually considered as a mixed valence oxide with pure spinel structure, in which nickel occupies octahedral position and cobalt distributes in octahedral and tetrahedral position. $NiCo_2O_4$ has the advantages of wide source, aplenty resources and friendly environment.[69] Compared with nickel oxides and cobalt oxides $NiCo_2O_4$ has more redox chemistry, better electronic conductivity and higher electrochemical activity than. Wang and co-workers[68] synthesized $NiCo_2O_4$ with typical aggregated porous morphology, large specific surface area (190.1 m^2 g^{-1}) and high mesoporous volume (0.943 cm^3 g^{-1}). TEM images shows the surface morphology and crystalline structure of as-synthesized $NiCo_2O_4$ materials (Figure 5a–b). Benefiting from the well-designed porous structure, the fabricated $NiCo_2O_4$ //AC hybrid NIC device exhibited energy and power densities (23.5 Wh kg^{-1} and 308 W kg^{-1}) and capacitive retention 61.2% after 2000 cycles (Figure 5c–d). However, its low conductivity and insufficient layer spacing for rapid insertion of sodium ions limits its electrochemical performance in NICs, which needs to be optimized in future researches.

3.2.2. Titanates

At low voltage (0.3 V vs. Na^+/Na), sodium can be intercalated/deintercalated in layered sodium titanate ($Na_2Ti_3O_7$), which enables it to apply for the battery type anode of NICs.[70] Dong et al.[58] synthesized $Na_2Ti_3O_7$ in situ growth on 1D CNT ($Na_2Ti_3O_7$@CNT) as anode material for NICs. Benefiting from the unique 1D nanostructure and the existence of pseudocapacitive charge storage mechanism. The obtained $Na_2Ti_3O_7$@CNT// PSC NIC delivered a maximum energy density of 58.5 Wh kg^{-1} and a maximum power density of 3000 W kg^{-1} with an excellent capacitive retention of 75% after 4000 cycles at 0.4 A g^{-1}. Yu and co-workers[59] prepared urchin-like $Na_2Ti_3O_7$ (Figure 6a–b) as anode and the PSC (Figure 6c) as cathode to fabricate a NIC, as shown in Figure 6d. Due to the rational designed urchin-like structure, the quasi-solid-state NIC exhibited excellent rate performance, as shown in Figure 6e. Moreover, the device delivered high energy and power densities (111.2 Wh kg^{-1}and 11200 W kg^{-1}) as well as an advanced cycle life (capacity retention of 86% after 3000 cycles) (Figure 6f). Other reported works with sodium titanate and its composites as anode in NICs are summarized in table 1.

3.2.3. Phosphate

Sodium metal phosphates with NASICON-type three-dimensional network structure, which enables sodium ions to diffuse rapidly in the 3D channels contained in their crystal structure, has been called sodium-ion superconductors. NASICON-structured PO_4-type materials, such as $NaTi_2(PO_4)_3$ and $Na_3V_2(PO_4)_3$, are applied for high-rate anodes of NICs, as shown in table 1. Due to the toxic of vanadium, $NaTi_2(PO_4)_3$ are more promising and practical.

$NaTi_2(PO_4)_3$ nanocages constructed by iso-oriented tiny nanocrystals with a mesoporous architecture have been synthesized and applied for anode materials in NICs by Wei et al.[62] (Figure 7a–c), exhibiting a large initial Coulombic efficiency of 94%. The prepared $NaTi_2(PO_4)_3$ nanocages illustrated outstanding rate capability (98 mA h g^{-1} at 10 C), and long cycling life (over 77% capacity retention after 10000 cycles) in half cells. The obtained hybrid $NaTi_2(PO_4)_3$//AC NIC

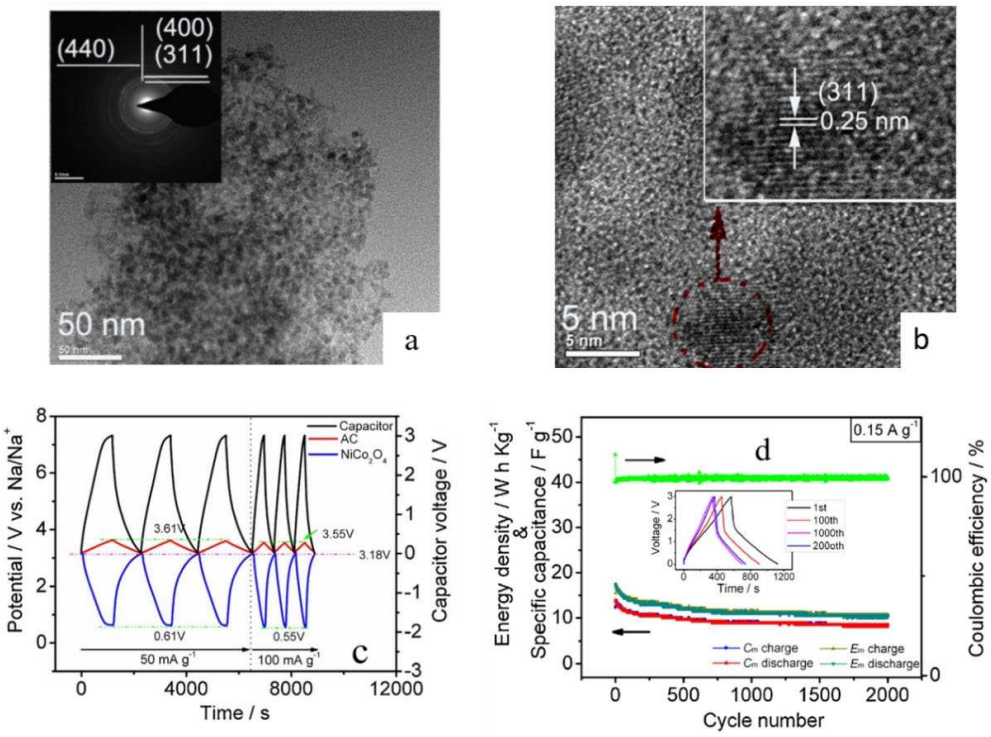

Figure 5. (a) TEM and (b) HRTEM images of $NiCo_2O_4$. (c) CP curves for the AC cathode and $NiCo_2O_4$ anode. (d) Cycling performance of the $NiCo_2O_4$/AC hybrid capacitor. Redrawn from Ref. [68].

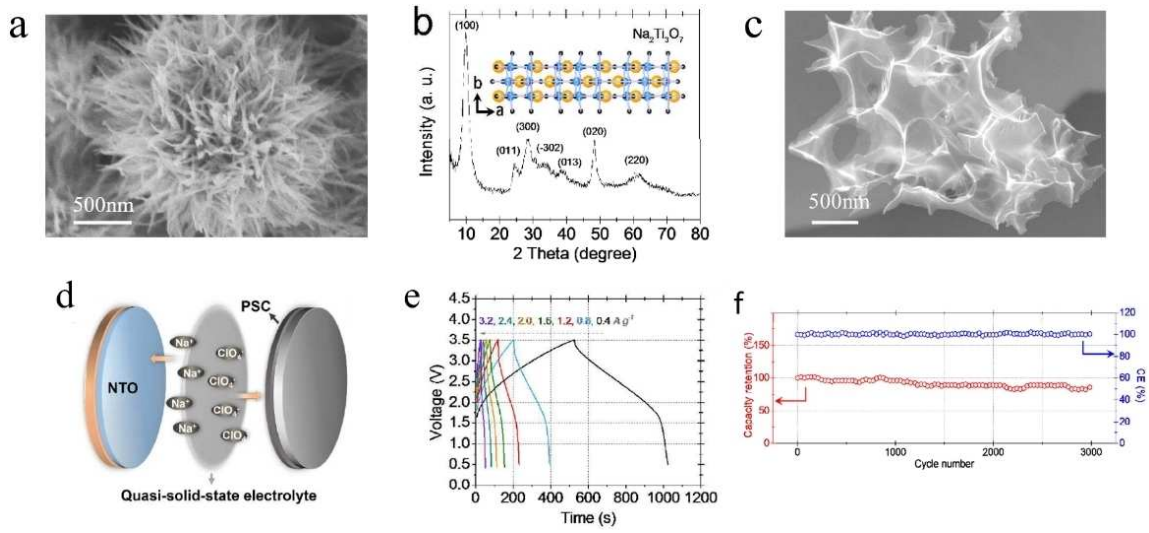

Figure 6. (a, b) SEM image and XRD patterns of urchin-like $Na_2Ti_3O_7$. (c) SEM image of PSC cathode material. (d) Schematic of a coin cell type sodium-ion capacitor. (e) Galvanostatic charge-discharge profiles at various current densities. (f) Cycling stability tested at 3.2 A g^{-1} for 3000 cycles. Redrawn from Ref. [59].

(Figure 7d) delivered an energy density of 56 Wh kg^{-1} at a power density of 39 W kg^{-1}, as well as, little capacity degradation after 20000 cycles at a high current rate of 5 A g^{-1} (as shown in Figure 7e–f).

In order to improve the conductivity of $NaTi_2(PO_4)_3$, Kim et al.[63] modified $NaTi_2(PO_4)_3$ by rGO with simple spray drying method. The obtained $NaTi_2(PO_4)_3$@rGO//AC NIC exhibited a high energy density of 53 Wh kg^{-1} and power density of 6680 W kg^{-1} due to the rational design of composite structure. Lee et al.[64] prepared $NaTi_2(PO_4)_3$ grown on graphene nanosheets as an intercalation electrode and 2D graphene nanosheets as an adsorption electrode. The fabricated $NaTi_2(PO_4)_3$@GNs//CNs hybrid NIC device exhibited a maximum energy density of 80 Wh kg^{-1} and a maximum power density of 8000 W kg^{-1}, with an excellent capacitive retention of 90% after 75000 cycles. Further reported works with Sodium metal phosphates (as shown in table 1) as anode also indicate that

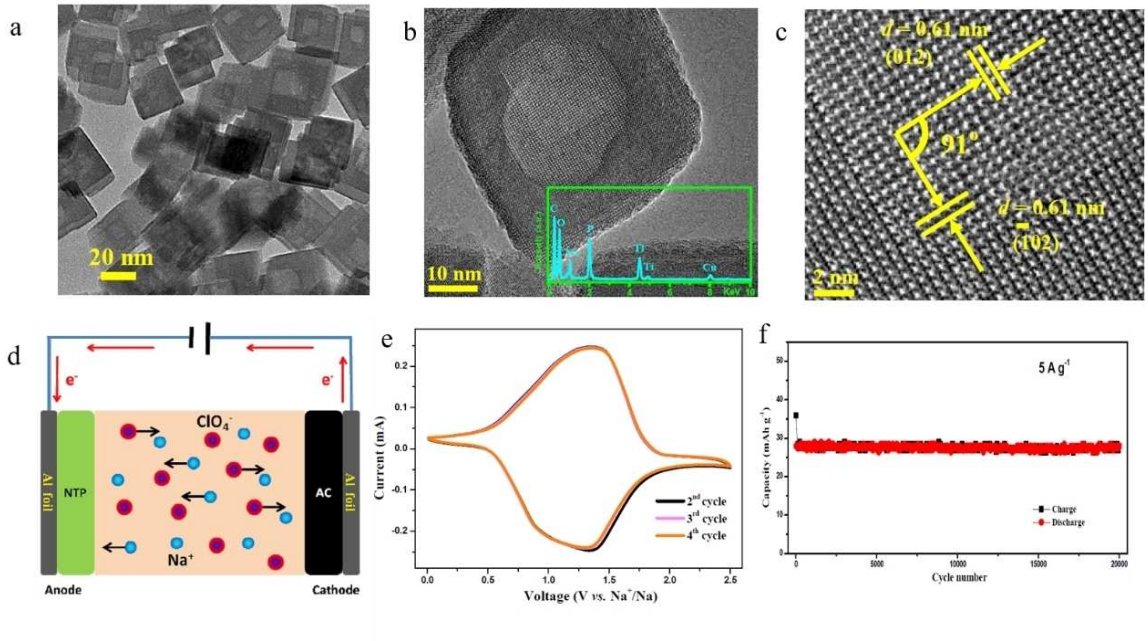

Figure 7. (a, b) TEM images. (c) HRTEM Image of NTP nanocages. (d) Schematic illustration of the operating mechanism of the NIC. (e) CV curves and (f) Long-term cycling performance of NIC. Reprinted from Ref. [62] with permission from American Chemical Society. Copyright (2017) American Chemical Society.

$NaTi_2(PO_4)_3$ is a suitable candidate for negative electrode of NICs.

3.3. Carbonaceous Materials

3.3.1. Hard Carbon

Hard carbon is kind of carbon materials with unique structure (Figure 8a–b), which normally obtained by paralyzing high-molecular polymer and decomposing a crosslinked block resin. As early as 2000s, hard carbon as an NIB anode was first reported and they had achieved a reversible sodium capacity of 300 mA h g^{-1}.[71] It has been used as an anode in NICs considering its abundant ion storage mechanism: (1) intercalation between graphene sheets in the turbostratic graphitic structures; (2) storage in the closed microspores; (3) surface and defect absorption.[72]

Goikolea and co-workers[73] pyrolyzed olive nucleus to obtain low specific surface area hard carbon as anode and further activated by KOH to obtain high SSA activated carbon as cathode for a NIC. The prepared hard carbon in organic sodium salt electrolyte showed reversible capacitance of 243 mA h g^{-1}. The resulted NIC demonstrated a maximum energy density of 100 Wh kg^{-1}, a maximum power density of 7000 W kg^{-1} and good cycling stability up to 5000 cycles with 70% capacity retention. Other reported NICs with hard carbon as anodes, such as sodium pre-doped hard carbon//AC showed considerable electrochemical performance.[74] However, limitations such as sensitive to polarization, poor rate capability and cycle performance are still remain, which causing by its low potential plateau. The hydrophilicity and conductivity of hard carbon materials can be improved by ion doping or composite method, which enable to enhance the energy storage performance of hard carbon materials in NICs.[75]

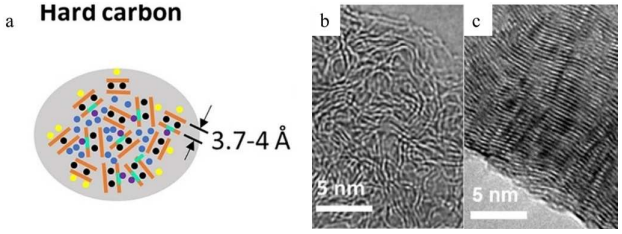

Figure 8. (a) Schematic illustrations of the ion storage in HC. HRTEM images of (b) hard carbon, (c) soft carbon. Redrawn from Ref. [71c, 77].

3.3.2. Soft Carbon

Differing from hard carbon, soft carbon usually comes from aromatic hydrocarbons, such as asphalt tar, petroleum, and coal refining with low oxygen content.[76] Soft carbon is amorphous non-graphitized carbon material with large interlayer spacing, which can be graphitized after being carbonized at a high temperature (about 2500 °C). When employed for sodium ions storage, soft carbon shows some unique advantages, such as good compatibility with electrolyte and no obvious charge and discharge platform. In contrast to hard carbon, soft carbon has higher conductivity. Moreover, soft carbon delivers a good capacity at potentials above 0.2 V when used as an anode in NICs. Han et al.[77] employed graphitic mesocarbon microbead as anode and activated carbon as

cathode for a NIC. The fabricated NIC device presents energy density of 93.5 Wh kg^{-1}, power density of 2832 W kg^{-1} and 98.3% capacity retention after 3000 cycles at 20 C with a wide voltage window of 1–4 V. Sodium ions can be reversibly embedded in the graphite anode in diglyme-based electrolyte, which contributes to the excellent electrochemical performance. Unfortunately, soft carbon has relatively low first-cycle columbic efficiency, cycle efficiency and stability. In addition, the graphite layer in soft carbon is better arranged than hard carbon, which limits the diffusion rate of sodium ions in bulk of electrode, as shown in Figure 8c.

3.4. MXene

As a novel family of nanosheet compounds, MXene is derived by etching $M_{n+1}AX_n$ phase or MAX with concentrated hydrofluoric acid, where M is an early transition metal, A is a third and fourth main group element and X is C or N. The MXene phase has high electrical conductivity (for example, 2.4×10^5 Sm^{-1} for $Ti_3C_2T_x$ film) and a large surface area.[78] MXene enables rapid ion motion and electron exchange and provides a large number of electrochemically active sites for redox reactions, ion adsorption and interactions. Combining the advantages mentioned above, the material is an ideal candidate as battery type anode for NICs.

Gogotsi et al.[79] reported bi-stacked 2D titanium carbide electrodes without binder, conductive additives and current-collector, showing good cycle stability and rate performance when employed to store sodium ions. With activated carbon as cathode, the fabricated NIC showed high energy and power densities (39 Wh kg^{-1} and 1140 W kg^{-1}) and good cycling stability (84.2% capacity retention after 4000 cycles). By a method of using cetyltrimethylammonium bromide (CTAB) pretreatment, thermal diffusion with elemental S, and followed annealing process, as shown in Figure 9, S atoms could be successfully intercalated into the interlayer of Ti_3C_2.[80] The as-obtained hybrid CT-S@Ti_3C_2-450//AC NIC delivers a high energy density of 263.2 Wh kg^{-1} at a high power density of 8240 W kg^{-1}, and outstanding cycling performance with 73.3% capacity retention after 10 000 cycles. It was also reported that MXenes materials, such as M-TiO_2-RGO,[41] Ti_2C,[81] Ti_3C_2/CNT,[82] Na-Ti_3C_2,[83] are applied for anodes in NICs, achieving good electrochemical performance.

The practical energy storage performance of MXene mainly depends on the properties of end groups. The -OH groups can increase the active sites for electrolyte ions, but reduce the reaction kinetics during charge and discharge due to the reduced ion diffusion rate. Through increase the interlayer spacing of MXene reasonably, such as sodium pillared[83] and doped atoms, the reaction kinetics could be enhanced effectively. Various battery-type anode materials including layered metal oxides, metal sulfides, metal salt and NASICON-type materials are summarized in table 1. It appears that the max energy densities of the most reported NICs are lower than 150 Wh kg^{-1}, which restricts the practical application of NICs On the other hand, the rate of Na^+ intercalates and deintercalates into the battery-type electrode is generally much slower than that of non-Faradaic capacitive charge storage. Therefore, improving the reaction kinetics of battery-type anode materials is crucial to enhance the electrochemical performance of NICs, especially for power density. In this case, diverse methods could be used to improve the reaction kinetics of battery-type anode materials: (1) Micro-nanocrystallization of the electrode material to increase the specific surface area of the material; (2) Shortening the diffusion distance; (3) Coating conductive polymers to improve rate performance.

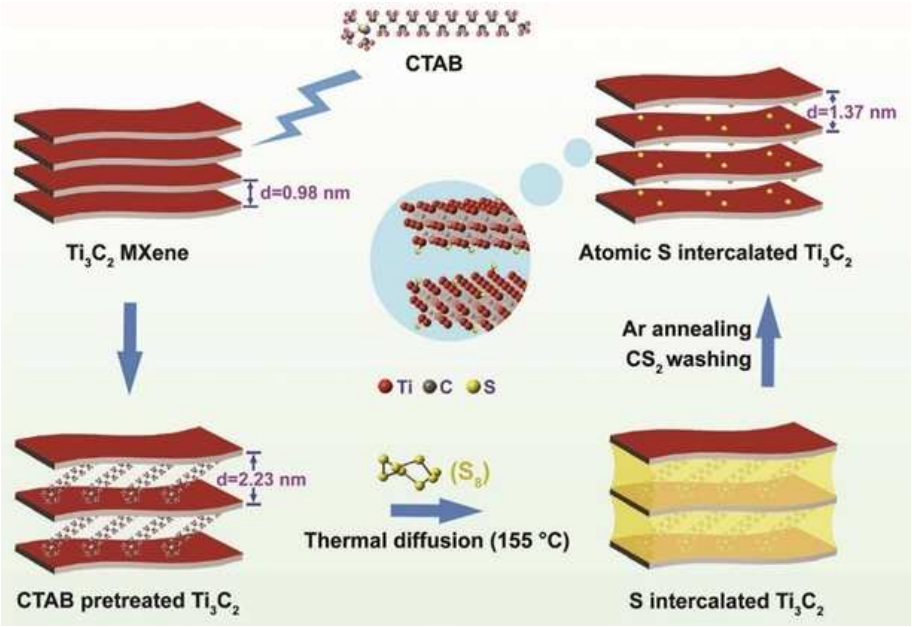

Figure 9. Schematic illustration of the synthesis of S atoms intercalated Ti_3C_2. Redrawn from Ref. [80].

4. Battery-Type Cathode Materials

Some battery type electrode materials with high redox potential can also be used as cathode for NICs with capacitive carbon materials as the anode. Typical cathode materials such as $Na_3V_2(PO_4)_3$,[84] ferric vanadate,[85] and $Na_{0.66}Mn_{0.5}4Ni_{0.13}Co_{0.13}O_2$ (NMNC)[86] has been reported to be applied for NICs with carbon materials as anode. With modified rationally, these battery-type cathode materials exhibited excellent electrochemical performance in NICs.

4.1. $Na_3V_2(PO_4)_3$

As a typical cathode material for sodium-ion batteries, $Na_3V_2(PO_4)_3$ (NVP) with a NASICON structure favors the insertion and extraction of Na^+. The NASICON structure features a highly covalent three-dimensional framework that generates large interstitial spaces through which sodium ions may diffuse. However, due to the crystal structure of NVP and low electron conductivity, theoretical capacity cannot be realized at high power. To solve this problem, modifying $Na_3V_2(PO_4)_3$ with highly conductive materials, such as carbon materials, are investigated to improve electrochemical performance. Xu et al.[84] reported N-doped mesoporous carbon nanosheets array uniformly encapsulated VO_2 (VO_2@mp-CNSs) as anode and $Na_3V_2(PO_4)_3$ nanoparticles (NVP@mp-CNSs) as cathode for NICs (Figure 10). Assembled VO_2@mp-CNSs//NVP@mp-CNSs NIC device delivered both high energy density (161 Wh kg^{-1}) and power density (24000 W kg^{-1}) as well as an advanced cycle stability (capacity retention: 78% at 1 A g^{-1} after 2000 cycles).

4.2. Ferric Vanadate

Layered ferric vanadate (FVO) normally exhibits large tunnels favoring for ion insertion which delivers a high reversible sodium storage capacity, excellent rate capability and cycling stability. During the early sodium ions storage researches FVO displayed excellent performance[87] as cathodes. Wei and co-workers[85] assembled a NIC device with FVO nanosheets as the cathode and hard carbon as anode. The storage mechanism of pseudocapacitive sodium in FVO was confirmed by kinetic analysis and ex situ characterization, in which capacitive sodium accounts for more than 83% of the total capacity. The assembled HC//FVO NIC delivered a maximum energy density of 194 Wh kg^{-1} and power density of 3942 W kg^{-1} and was capable of working under a wide potential range of 0–3.8 V with 89% capacity retention after 1000 cycles. This work highlights the advantages of the pseudo-capacitive cathode in sodium storage performance.

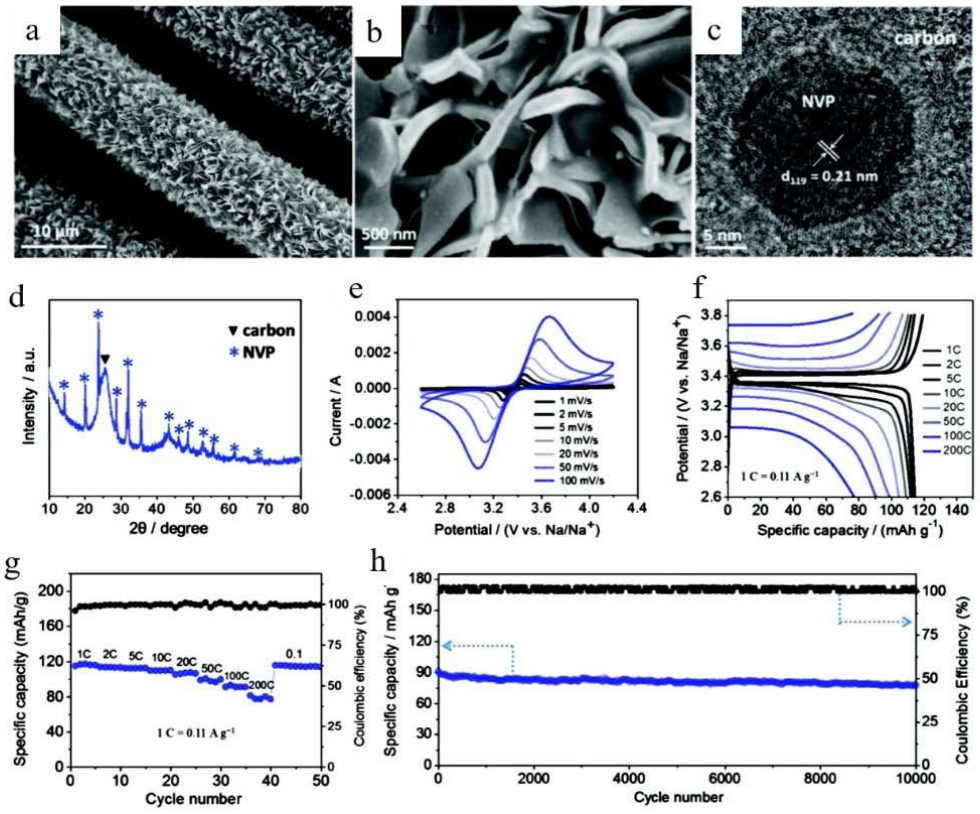

Figure 10. (A, B) FESEM, (C) TEM, (D) XRD pattern of NVP@mp-CNSs. (E) CV curves, (F) charging/discharging curves, (G) rate performance and (H) cycling performance of the NVP@mp-CNSs sample. Redrawn from Ref. [84].

4.3. $Na_{0.66}Mn_{0.54}Ni_{0.13}Co_{0.13}O_2$ (NMNC)

Kaliyappan et al.[86] fabricated a NIC with an Al_2O_3-coated NMNC (NMNC-Al) as an cathode and a commercial activated carbon (CAC) as the anode materials. The reaction mechanism of NMNC electrode is described as:

$$\text{Cathode}: Na_{0.66}\ (Mn_{0.54}{}^{3+}Ni_{0.13}{}^{2+}Co_{0.13}{}^{3+})\ O_2 \Leftrightarrow Na_{0.66-x}\ (Mn_{0.54}{}^{4+}Ni_{0.13}{}^{3+}Co_{0.13}{}^{4+})\ O_2 + x\ Na^+ + x\ e^- \quad (1)$$

$$\text{Anode}: AC + x\ e^- \Leftrightarrow AC(x\ e^-) + //ClO_4{}^- \quad (2)$$

(//stands for double layer)

Generally, Na^+ are deintercalated from the NNMC structure and infused into the electrolyte solution while the electrons flow to the external circuit during the charging process. In the charging process Na^+ are intercalated into the NNMC electrode from the electrolyte. In terms of CAC anode, ClO_4^- also are adsorbed and desorbed on the interface between electrolyte and electrode, thus forming the electrical double layer (EDL) during the charge/discharge process. Combining the high energy density resulted from Na^+ intercalation/deintercalation into NNMC and the essential power density from EDL on the CAC electrode surface, the obtained CAC//NMNC–Al NIC delivered a discharge capacity of 66 F g^{-1}, energy density of 75 Wh kg^{-1} at the power density of 2.23 kW kg^{-1}.remarkably, the NIC device also demonstrated an extremely stable cyclic stability of 98% after 10,000 cycles. Further reported works with battery-type cathode are shown in table 2. The max energy density of listed NICs are below 75 Wh kg^{-1}. Interestingly, some NICs devices employ Na_2SO_4 and NaOH aqueous solution as electrolyte instead of organic solution. The NICs with aqueous electrolyte normally safer than organic counterpart, but their energy densities are much lower due to narrow potential window.

5. Dual-Carbon NIC

Metal-contained compounds normally harm to the environment during producing and usage. In a typical dual-carbon NIC, carbon materials which allows Na^+ intercalation and deintercalation reversibly, such as hard carbon, are employed as battery-type anode, while carbon materials with high specific surface area and widely distributed pores, such as activated carbon, are applied for capacitor-type cathode.[94] Remarkably, some carbon materials could meet the needs for battery-type anode and capacitor-type cathode simultaneously, delivering both high reversible redox capacity and high capacity with EDL. In this case, these unique carbon materials can be applied for anode and cathode simultaneously, assembling a symmetrical NIC.[95]

Considering the fact, Wang and co-workers[95a] synthesized peanut skin-derived carbon nanosheets (PSC) and used as both cathode and anode electrode for NICs. The obtained carbon had a hierarchical microporous-mesopor-macroporous disorder structure, which facilitates the rapid transport of electrolyte ions. In addition, the rich defect sites could increase the sodium storage capacity of the material. When used as an anode for sodium ions storage, the PSC electrode indicated a specific capacity of 461 mA h g^{-1} at 100 mA g^{-1} and excellent rate capability. The fabricated NICs hybrid device exhibited a maximum energy and power densities (112 Wh kg^{-1} and 12,000 W kg^{-1}) with an excellent capacitive retention of 85% after 3000 cycles. Cathode based on Peanut Shell Nanosheet Carbon (PSNC), with hierarchically porous architecture sheet-like morphology, as shown in Figure 11a, and a low surface area Peanut Shell Ordered Carbon (PSOC) as ion intercalation anode, (Figure 11b) are employed for a NIC.[96] The assembled PSNC-3-800//PSOC-A NIC device indicated high energy and power densities (201 Wh kg^{-1} and 30000 W kg^{-1}) with good cycling stability (88% capacity retention after 10,000 cycles) (Figure 11f).

Table 2. Performance of NICs composed of battery-type cathode.

Anode/Cathode	electrolyte	Potential range [V]	Max energy density [Wh kg^{-1}]	Max power density [W kg^{-1}]	Cycling life	Year	Ref.
Graphene/Ni-HCF	1 M Na_2SO_4	0–2	39.35	3333.33	91%@1 A/g after 2k cycles	2017	[88]
CMS/Co HCF	0.5 M Na_2SO_4	0–2	54.4	5037	92%@2 A/g after 1k cycles	2016	[89]
AC//Na_2CoSiO_4	2 M NaOH	0–0.45	12.4	2000	84%@1 A/g after 1.5k cycles	2015	[90]
Ti_2C-MXene//$Na_2Fe_2(SO_4)_3$	1 M $NaPF_6$ (EC/DEC)	0.1–3.8	320	1440	96%@0.6 A/g after 0.1k cycles	2015	[81]
AC//$Na_3V_2(PO_4)_3$/C	0.5 M Na_2SO_4	0–1.5	15.93	750	80% after 0.1k cycles	2015	[91]
AC//PB	0.5 M Na_2SO_4	0–1.8	30	1193	97%@0.5 A/g after 1.1k cycles	2016	[92]
HC//Fe–V-O	1 M $NaPF_6$ (Diglyme)	0–3.8	194	3942	89% after 1k cycles	2018	[85]
AC//$Na_{0.44}MnO_2$	1 M $NaClO_4$	0–2.7	17.5	4750	85% after 1k cycles	2018	[12a]
ZDC//P2-NCM	1 M $NaClO_4$ (EC/PC)	0-3	18.8	12750	80%@5 A/g after2k cycles	2019	[93]
CAC//$Na_{0.66}Mn_{0.54}Ni_{0.13}Co_{0.13}O_2$	1 M $NaClO_4$ (EC/DEC)	0–3	75	2230	98%@0.35 A/g after 10k cycles	2018	[86]
VO_2@mp-CNSs//NVP@mp-CNSs	1 M $NaClO_4$ (PC/FEC)	1–4	161	24000	78%@1 A/g after 2k cycles	2018	[84]

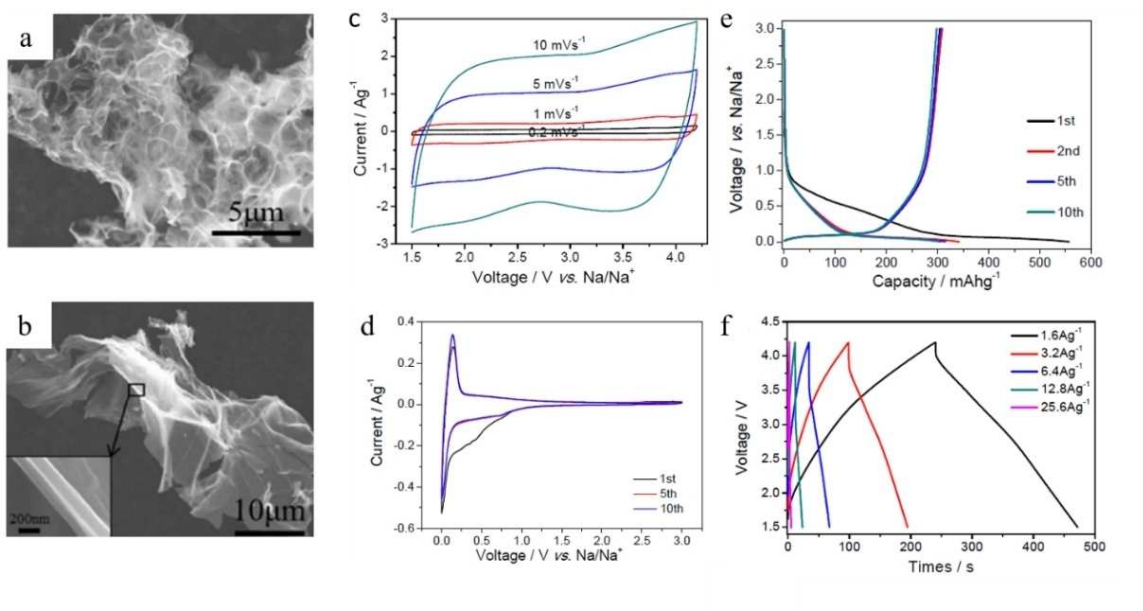

Figure 11. SEM image of (a) PSNC-3-800 and (b) PSOC-A. Cyclic voltammograms (CVs) of (c) PSNC-3-800 and (d) PSOC-A. (e) Galvanostatic discharge/charge profiles of (e) PSOC-A and (f) PSNC-3-800//PSOC-A. Redrawn from Ref. [96].

In order to further improve the performance of dual-carbon NICs, a method based on citrate as the precursor has been proposed to prepare thin carbon materials with three-dimensional structure, wide interlayer spacing and high electrical conductivity. Yang et al.[97] prepared three-dimensional carbon materials (3DFCs) by using sodium citrate as the sole precursor without any additional template or catalyst. The three-dimensional structure promotes rapid insertion/extraction. The electrode exhibited a highly reversible capacity (333 $mA\,h\,g^{-1}$ at 0.05 $A\,g^{-1}$), excellent magnification and cyclic performance (at 10 $A\,g^{-1}$, 1000 $mA\,h\,g^{-1}$) after 1000 cycles. After activated by KOH, 3DFCs gave high SSA of 1094 $m^2\,g^{-1}$ with rich mesoporous structure. The activated 3DFC (3DFAC) demonstrated a specific capacity of 71.3 $mA\,h\,g^{-1}$ in the potential window of 2.5–4.2 V. The fabricated 3DFCs//3DFAC hybrid device exhibited a maximum energy density of 200 $Wh\,kg^{-1}$ and a maximum power density of 20000 $W\,kg^{-1}$ with an excellent capacitive retention of 80% after 10000 cycles in the voltage range of 0–4 V.

Carbon microspheres with regular geometry, non-graphite properties and stability properties are promising candidates for NICs, but their synthetic methods are often complex and energy intensive. Wang and co-workers[94a] reported a non-purified strategy to synthesize carbon microspheres directly from five fresh juices. The synthesized carbon microspheres exhibited an expanded interlayer distance of 0.375 nm, which promotes the absorption and release of Na^+ during charge and discharge. A NIC assembled with activated carbon microsphere cathode, illustrated a working voltage 0–4 V, maximum energy density of 52.2 $Wh\,kg^{-1}$, power density up to 3000 $W\,kg^{-1}$ and capacity retention of 85.7% after 2000 cycles. By easy activation highly porous carbon microsphere positive electrodes are produced and exhibited a much higher energy density at higher rates than commercial activated carbon.

The surface oxygen-functionalized wrinkle graphene has a dense and porous structure, which ensures the active site of sodium-ion richness and shortens the ion diffusion path. Dong and co-workers[98] employed oxygen-functionalized crumpled graphene (OCG) as both the battery-type anode and capacitor-type cathode for a NIC. The symmetrical dual-carbon NIC exhibited high energy and power densities (121.3 $Wh\,kg^{-1}$ and 8000 $W\,kg^{-1}$) as well as an advanced cycle life (capacity retention of 86.7% after 25000 cycles).

The reported work about dual-carbon NICs and corresponding performance parameters are listed in Table 3. The energy densities of .dual-carbon NICs are generally above 100 $Wh\,kg^{-1}$. With metal-free and reproducible carbon materials as both anode and cathode, the energy density and power density are obviously increased, considering the low cost and environmentally-friend dual-carbon NICs are promising candidates for next-generation energy storage device.

The type and concentration of electrolyte are crucial to the electrochemical performance in NICs, considering the match to electrode materials. Thus, electrolyte should be carefully selected to the different NICs. For all reported battery-type anode and some battery-type cathode NICs, $NaClO_4$ or $NaPF_6$ dissolved in organic solvent (EC, PC, EMC, DMC, DEC, FEC or their mixture) are employed as electrolyte. For some part battery-type cathode NICs, NaOH or Na_2SO_4 aqueous solution are used as electrolyte. In addition, the formation speed of solid electrolyte interface (SEI) are affected by the electrolyte. Furthermore, some electrolyte would corrode the active materials, which results in the decline of electrochemical performance.

Table 3. Performance of NICs composed of Dual-carbon Materials.

Anode//Cathode[ref]	electrolyte	Potential range [V]	Max energy density [Wh kg^{-1}]	Max power density [W kg^{-1}]	Cycling life	Year	Ref.
Hard carbon//H-NPS	1 M $NaClO_4$ (EC/PC)	1.2–4.4	217	1900	3k cycles	2016	[99]
NHTC//APDC	1 M $NaClO_4$ (EC/DMC)	1.5–3.5	133	14250	82.5 %@2 A/g after 12k cycles	2018	[100]
Olive pit based HC//AC	1 M $NaPF_6$ (EC/PC)	1.5–4.2	100	7000	70 %@2 A/g after 5k cycles	2017	[73]
Graphitic mesocarbon microbead//AC	1 M $NaPF_6$ (Diglyme)	1–4	93.5	2832	98.3 %@20 C after 3k cycles	2015	[77]
Soft carbon//N-doped HC	1 M $NaPF_6$ (EC/DMC)	0.01–4.7	245.7	1626	1k cycles	2018	[101]
Disordered carbon nanoparticles// N-doped carbon hollow microspheres	1 M $NaPF_6$	0–4.4	157		70 %@0.3 A/g after 1k cycles	2017	[102]
Sodium pre-doped HC//AC	1 M $NaPF_6$ (EC/DEC)	1.5–4			91 % after 1k cycles	2012	[74]
SCN–A// SCN-A	1 M $NaClO_4$ (EC/DEC)	0–4	112	12000	85 %@5 A/g after 3k cycles	2016	[95a]
PSCN-3-800//PSOC-A	1 M $NaClO_4$ (EC/DEC)	1.5–3.5	201	16500	88 %@51.2 A/g after 100k cycles	2015	[96]
3DFC//3DFC-derived nanoporous carbon	1 M $NaClO_4$ (EC/DMC)	0–4	110	20000	80 %@2 A/g after 10k cycles	2018	[97]
CS-800//CS-800-6	1 M $NaClO_4$ (EC/DEC)	0–4	52.2	3000	85.7 %@1 A/g after 2k cycles	2018	[94a]
OCG//OCG	1 M $NaClO_4$ (EC/DEC)	0.5–3.5	121.3	8000	86.7 %@0.5 A/g after 2.5k cycles	2018	[98]
NOFC//PSNC	1 M $NaClO_4$ (EC/DEC)	2.7–4.2	111	14550	90 %@6.4 A/g after 5k cycles	2016	[94b]
EDHPC//EDHPC	1 M $NaClO_4$ (EC/DEC)	0–4	84	9053	67 %@10 A/g after 5k cycles	2018	[95b]
AHC//AHC	1 M $NaClO_4$ (EC/DMC)	1.5–4.2	43	3724	@2 A/g after 5k cycles	2018	[103]
HPC-550//HPC-800	1 M $NaClO_4$ (EC/EMC/FEC)	0–4	103.2	15900	81.1 %@3.5 A/g after 2.5k cycles	2019	[104]

For the quick index, Figure 12 propose a simple performance maps for the electrochemical properties including max power density and max energy density of the different type electrode, in which black points refers to NICs with battery-type anodes, red points to NICs with battery-type cathode and blue points to dual-carbon NICs. the major max energy densities of NICs with battery-type anodes range from 40–100 Wh kg^{-1}, while the corresponding max power densities from 1000 W kg^{-1} to 25000 W kg^{-1}. In contrast, the max energy and power densities of NICs with battery-type cathode are extremely dispersive. Remarkably, the dual-carbon NICs exhibit most concentrative max energy and power densities, mostly ranging from 100 Wh kg^{-1} to 200 Wh kg^{-1} for energy densities and from 2000 W kg^{-1} to 20000 W kg^{-1} for power densities. The value dispersion may not reflect the real quality of the materials since these data from references collected under different conditions.

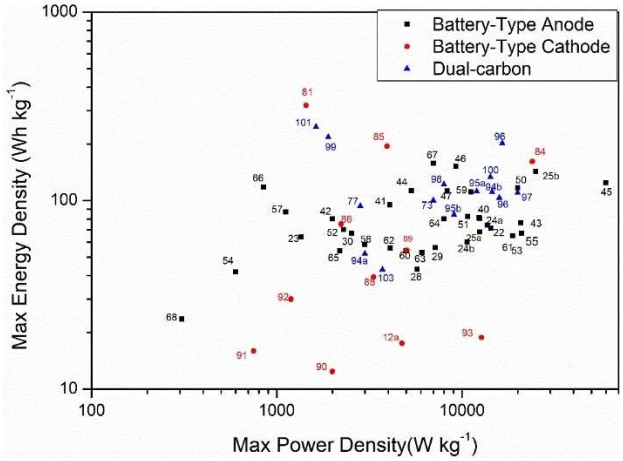

Figure 12. Performance comparisons of reported NIC devices.

6. Conclusion and Outlook

Sodium-ion capacitors integrate high-energy batteries and high-power capacitors have drawn considerable attentions. To match the fast kinetics of the capacitive electrode, the improvement of the high-rate capability is essential for battery-type electrode. Metal oxides including various polymorphs of titanium dioxide (TiO_2), Niobium pentoxide (Nb_2O_5) intensively used as anode electrode material in NICs due to those abundant reserves, stable structure, low price. Though very low volume expansion of the lattice makes that metal oxides has an advantage in cycling stability. The issue of low capacity may solve by controlling the particle size to nano dimension to shorten the Na-diffusion path, and hence increases the ionic diffusivity. Metal sulfides including non-layered sulfides (FeS, FeS_2 Sb_2S_3) and layered disulfides (SnS_2, MoS_2), usually have

better electrical conductivity, mechanical properties, thermal stability and rich redox chemistry than metal oxide. Layered disulfides benefited from large interlayer spacing that not only facilitates the insertion and extraction of sodium ion, but also serves as the buffer area to alleviate the volumetric variation. However, the inactive components including binder, conductive additive and current collector lower the layer structure ratio which decreases the energy density. Development on self-supporting layered disulfides electrodes may make this kind materials apply to the NIC realistically. As a typical metal salts, $NiCo_2O_4$ has more redox chemistry, better electronic conductivity and higher electrochemical activity than nickel oxides and cobalt oxides. Some Na compounds including NVP, FVO and NMNC-Al. etc present higher voltage as well as higher energy density. Considering the numbers of Na compounds are about twice than Li compounds, the possibility of Na compounds in real application on NICs electrode deserve further development. Carbonaceous materials including hard carbon and soft carbon are environmentally friendly and resourceful. Ion doping, composite with complementary materials, control of interlayer spacing and microporous structure would be targeted modification methods for its performance improvement. Although, the layered structure of MXene is main reason of its high specific capacity. The end group of MXene, in another hand, can increase the active sites for ions effectively. Thus, doping of ions and development of novel element MXene to increase interlayer space and modify end group would be effective approach to improve its reaction kinetics. Dual-carbon NIC, provides an possibility to compose a NIC without metal element. This is an important attribute in the context of that environmental and resource issues keep highlighting. Not to mention its rather high energy density and power density.

Although solid progress on battery type electrode for NICs have been made in the past few years. Still there are plenty of issues yet to be solved. For instance, the large volume expansion of anode during the insertion of sodium ions with larger radius causes low recyclability. The abandon metal contained electrode causes potential environmental and resource problems. Binders that commonly used to integrate individual active materials with conductive additives are reduces the overall energy density and leads to poor cycling stability since the necessary evil followed block the active sites, inhibit diffusion, and increase the electron transfer resistance. In view of the above problems, nanostructure and crystal structure adjusting including anion-doping strategy to form heterostructure, template inducing to control hollow structure and even multi-phase carbon matrix composites .etc may be effective solution. Furthermore, the use of organic materials with porous structure may also offer unique opportunity that integrates high capacity, fast diffusion rate, and structure stability into one material that can balance stability and performance. On the other, to design binder-free electrodes by directly growing the active material on a current collector or assisted by templates is suggested to expose more active sites and then provide possibility for high-performance NICs in terms of both improved conductivity and reversibility.

Acknowledgements

This work was financially supported by the Natural Science Foundation of Tianjin Municipality (18JCYBJC21200), the National Natural Science Foundation of China (NSFC. 21503146), and Yangtze Scholars and Innovative Research Team in Chinese University (IRT-17R81).

Conflict of Interest

The authors declare no conflict of interest.

Keywords: sodium-ion hybrid capacitors · electrode materials · energy-power density · energy storage

[1] a) J. Li, Q. Q. Jiang, N. N. Yuan, J. G. Tang, *Materials* **2018**, *11*, 2280; b) D. X. He, A. J. Marsden, Z. L. Li, R. Zhao, W. D. Xue, M. A. Bissett, *J. Electrochem. Soc.* **2018**, *165*, A3481–A3486; c) Y. L. An, H. F. Fei, J. K. Feng, L. J. Ci, S. L. Xiong, *Funct. Mater. Lett.* **2016**, *9*, 1642008.
[2] a) H. Hou-Sheng, C. Kuo-Hsin, S. Norihiro, Y. Yusuke, H. Chi-Chang, W. Kevin C.-W. *Small* **2013**, *9*, 2520–2526; b) C. Young, J. Wang, J. Kim, Y. Sugahara, J. Henzie, Y. Yamauchi, *Chem. Mater.* **2018**, *30*, 3379–3386.
[3] R. R. Salunkhe, Y. H. Lee, K. H. Chang, J. M. Li, P. Simon, J. Tang, N. L. Torad, C. C. Hu, Y. Yamauchi, *Chem. Eur. J.* **2014**, *20*, 13838–13852.
[4] a) X. N. Feng, M. G. Ouyang, X. Liu, L. G. Lu, Y. Xia, X. M. He, *Energy Storage Mater.* **2018**, *10*, 246–267; b) W. P. Kang, Y. Y. Wang, J. Xu, *J. Mater. Chem. A* **2017**, *5*, 7667–7690; c) S. P. Guo, J. C. Li, Z. Ma, Y. Chi, H. G. Xue, *J. Mater. Sci.* **2017**, *52*, 2345–2355; d) X. Y. Wang, L. Fan, D. C. Gong, J. Zhu, Q. F. Zhang, B. G. Lu, *Adv. Funct. Mater.* **2016**, *26*, 1104–1111; e) J. H. Zhang, M. Huang, B. J. Xi, K. Mi, A. H. Yuan, S. L. Xiong, *Adv. Energy Mater.* **2018**, *8*, 1701330.
[5] a) J. J. Ye, Z. Z. Chen, Q. Liu, C. X. Xu, *J. Colloid Interface Sci.* **2018**, *516*, 1–8; b) S. Fleischmann, D. Leistenschneider, V. Lemkova, B. Kruener, M. Zeiger, L. Borchardt, V. Presser, *Chem. Mater.* **2017**, *29*, 8653–8662.
[6] a) R. R. Salunkhe, J. Tang, N. Kobayashi, J. Kim, Y. Ide, S. Tominaka, J. H. Kim, Y. Yamauchi, *Chem. Sci.* **2016**, *7*, 5704–5713; b) R. R. Salunkhe, Y. V. Kaneti, Y. Yamauchi, *ACS Nano* **2017**, *11*, 5293–5308.
[7] Y. Ouyang, H. Ye, X. Xia, X. Jiao, G. Li, S. Mutahir, L. Wang, D. Mandler, W. Lei, Q. Hao, *J. Mater. Chem. A* **2019**, *7*, 3228–3237.
[8] a) K. Zhang, X. W. Yang, D. Li, *J. Energy Chem.* **2018**, *27*, 1–5; b) J. Fei, Y. L. Cui, J. Y. Li, Z. W. Xu, J. Yang, R. Y. Wang, Y. Y. Cheng, J. F. Huang, *Chem. Commun.* **2017**, *53*, 13165–13167.
[9] G. G. Amatucci, F. Badway, A. Du Pasquier, T. Zheng, *J. Electrochem. Soc.* **2001**, *148*, A930–A939.
[10] J. Yin, L. Qi, H. Wang, *ACS Appl. Mater. Interfaces* **2012**, *4*, 2762–2768.
[11] a) Z. Chen, V. Augustyn, X. L. Jia, Q. F. Xiao, B. Dunn, Y. F. Lu, *ACS Nano* **2012**, *6*, 4319–4327; b) R. Thangavel, K. Kaliyappan, D. U. Kim, X. Sun, Y. S. Lee, *Chem. Mater.* **2017**, *29*, 7122–7130.
[12] a) K. Wasinski, P. Polrolniczak, M. Walkowiak, *Electrochim. Acta* **2018**, *259*, 850–854; b) F. Yu, Z. C. Liu, R. W. Zhou, D. M. Tan, H. X. Wang, F. X. Wang, *Mater. Horiz.* **2018**, *5*, 529–535.
[13] Y. Fang, X. Y. Yu, X. W. Lou, *Angew. Chem. Int. Ed.* **2019**, *58*, 7744–7748.
[14] Y. J. Fang, X. Y. Yu, X. W. Lou, *Angew. Chem. Int. Ed.* **2018**, *57*, 9859–9863; *Angew. Chem.* **2018**, *130*, 10007–10011.
[15] P. L. He, Y. J. Fang, X. Y. Yu, X. W. Lou, *Angew. Chem. Int. Ed.* **2017**, *56*, 12202–12205; *Angew. Chem.* **2017**, *129*, 12370–12373.
[16] Y. Liu, Y. J. Fang, Z. W. Zhao, C. Z. Yuan, X. W. Lou, *Adv. Energy Mater.* **2019**, *9*, 1803052.
[17] B. P. Bastakoti, H. S. Huang, L. C. Chen, K. C.-W. Wu, Y. Yamauchi, *Chem. Commun.* **2012**, *48*, 9150–9152.
[18] J. Wang, J. Tang, B. Ding, V. Malgras, Z. Chang, X. D. Hao, Y. Wang, H. Dou, X. G. Zhang, Y. Yamauchi, *Nat. Commun.* **2017**, *8*, 15717.
[19] J. J. Liang, C. C. Yuan, H. H. Li, K. Fan, Z. X. Wei, H. Q. Sun, J. M. Ma, *Nano-Micro Lett.* **2018**, *10*, 21.
[20] X. Liu, N. Zhang, J. F. Ni, L. J. Gao, *J. Solid State Electrochem.* **2013**, *17*, 1939–1944.

[21] K. T. Kim, G. Ali, K. Y. Chung, C. S. Yoon, H. Yashiro, Y. K. Sun, J. Lu, K. Amine, S. T. Myung, *Nano Lett.* **2014**, *14*, 416–422.
[22] S. N. Liu, Z. G. Luo, G. Y. Tian, M. N. Zhu, Z. Y. Cai, A. Q. Pan, S. Q. Liang, *J. Power Sources* **2017**, *363*, 284–290.
[23] Z. Y. Le, F. Liu, P. Nie, X. R. Li, X. Y. Liu, Z. F. Bian, G. Chen, H. B. Wu, Y. F. Lu, *ACS Nano* **2017**, *11*, 2952–2960.
[24] a) S. N. Liu, Z. Y. Cai, J. Zhou, A. Q. Pan, S. Q. Liang, *J. Mater. Chem. A* **2016**, *4*, 18278–18283; b) D. Bauer, A. J. Roberts, S. G. Patnaik, D. J. L. Brett, P. R. Shearing, E. Kendrick, N. Matsumi, J. A. Darr, *J. Electrochem. Soc.* **2018**, *165*, A1662–A1670.
[25] a) B. Babu, S. G. Ullattil, R. Prasannachandran, J. Kavil, P. Periyat, M. M. Shaijumon, *ACS Sustainable Chem. Eng.* **2018**, *6*, 5401–5412; b) H. X. Li, J. W. Lang, S. L. Lei, J. T. Chen, K. J. Wang, L. Y. Liu, T. Y. Zhang, W. S. Liu, X. B. Yan, *Adv. Funct. Mater.* **2018**, *28*, 1800757.
[26] L. M. Wu, D. Bresser, D. Buchholz, G. A. Giffin, C. R. Castro, A. Ochel, S. Passerini, *Adv. Energy Mater.* **2015**, *5*, 1401142.
[27] H. Kim, E. Lim, C. Jo, G. Yoon, J. Hwang, S. Jeong, J. Lee, K. Kang, *Nano Energy* **2015**, *16*, 62–70.
[28] H. S. Li, Y. Zhu, S. Y. Dong, L. F. Shen, Z. J. Chen, X. G. Zhang, G. H. Yu, *Chem. Mater.* **2016**, *28*, 5753–5760.
[29] Z. Q. Tong, S. K. Liu, Y. Zhou, J. P. Zhao, Y. P. Wu, Y. S. Wu, Y. Li, *Energy Storage Mater.* **2018**, *13*, 223–232.
[30] Y. Q. Long, J. Yang, X. Gao, X. N. Xu, W. L. Fan, S. F. Hou, Y. T. Qian, *ACS Appl. Mater. Interfaces* **2018**, *10*, 10945–10954.
[31] Y. Fang, B. Y. Guan, D. Luan, X. W. Lou, *Angew. Chem. Int. Ed.* **2019**, *58*, 7739–7743.
[32] a) Y. H. Xue, Q. Zhang, W. J. Wang, H. Cao, Q. H. Yang, L. Fu, *Adv. Energy Mater.* **2017**, *7*, 1602684; b) P. Ge, H. S. Hou, C. E. Banks, C. W. Foster, S. J. Li, Y. Zhang, J. Y. He, C. Y. Zhang, X. B. Ji, *Energy Storage Mater.* **2018**, *12*, 310–323.
[33] N. Chen, C. P. Han, R. Y. Shi, L. Xu, H. F. Li, Y. S. Liu, J. Q. Li, B. H. Li, *Electrochim. Acta* **2018**, *283*, 36–44.
[34] Y. Z. Li, H. W. Wang, L. B. Wang, R. Wang, B. B. He, Y. S. Gong, X. L. Hu, *Energy Storage Mater.* **2019**, https://doi.org/10.1016/j.ensm.2019.05.024
[35] a) J. F. Ni, Z. Yang, L. Liang, L. Q. Mai, *Nano Energy* **2015**, *11*, 129–135; b) L. Guo, Y. Wang, *J. Mater. Chem. A* **2015**, *3*, 4706–4715.
[36] S. Hu, F. Yin, E. Uchaker, W. Chen, M. Zhang, J. Zhou, Y. Y. Qi, G. Z. Cao, *J. Phys. Chem. C* **2014**, *118*, 24890–24897.
[37] K. Ramakrishnan, C. Nithya, R. Karvembu, *ACS Appl. Energy Mater.* **2018**, *1*, 841–850.
[38] R. Kiruthiga, C. Nithya, R. Karvembu, B. V. R. Reddy, *Electrochim. Acta* **2017**, *256*, 221–231.
[39] Y. J. Fang, X. Y. Yu, X. W. Lou, *Adv. Mater.* **2018**, *30*, 1706668.
[40] Y. E. Zhu, L. P. Yang, J. Sheng, Y. A. Chen, H. C. Gu, J. P. Wei, Z. Zhou, *Adv. Energy Mater.* **2017**, *7*, 1701222.
[41] R. T. Wang, S. J. Wang, Y. B. Zhang, D. D. Jin, X. Y. Tao, L. Zhang, *J. Mater. Chem. A* **2018**, *6*, 1017–1027.
[42] H. Chen, C. L. Dai, Y. A. Li, R. M. Zhan, M. Q. Wang, B. S. Guo, Y. Q. Zhang, H. Liu, M. W. Xu, S. J. Bao, *J. Mater. Chem. A* **2018**, *6*, 24860.
[43] E. Lim, C. Jo, M. S. Kim, M. H. Kim, J. Y. Chun, H. Kim, J. Park, K. C. Roh, K. Kang, S. Yoon, J. Lee, *Adv. Funct. Mater.* **2016**, *26*, 3711–3719.
[44] X. G. Wang, Q. C. Li, L. Zhang, Z. L. Hu, L. H. Yu, T. Jiang, C. Lu, C. G. Yan, J. Y. Sun, Z. F. Liu, *Adv. Mater.* **2018**, *30*, 1800963.
[45] Y. Li, H. Wang, L. Wang, Z. Mao, R. Wang, B. He, Y. Gong, X. Hu, *Small* **2019**, *15*, 1804539.
[46] X. Hu, Y. J. Liu, J. X. Chen, J. C. Jia, H. B. Zhan, Z. H. Wen, *J. Mater. Chem. A* **2019**, *7*, 1138–1148.
[47] Y. Z. Li, H. W. Wang, B. J. Huang, L. B. Wang, R. Wang, B. B. He, Y. S. Gong, X. L. Hu, *J. Mater. Chem. A* **2018**, *6*, 14742–14751.
[48] Y. X. Wang, S. L. Chou, D. Wexler, H. K. Liu, S. X. Dou, *Chem. Eur. J.* **2014**, *20*, 9607–9612.
[49] R. Kiruthiga, C. Nithya, R. Karvembu, *Nanoscale Advances* **2019**, *1*, 1–11.
[50] K. Liao, H. W. Wang, L. B. Wang, D. M. Xu, M. Wu, R. Wang, B. B. He, Y. S. Gong, X. L. Hu, *Nanoscale Advances* **2019**, *1*, 1746–1756.
[51] X. Zhao, W. Cai, Y. Yang, X. D. Song, Z. Neale, H. E. Wang, J. H. Sui, G. Z. Cao, *Nano Energy* **2018**, *47*, 224–234.
[52] X. Zhao, Y. D. Zhao, Z. Liu, Y. Yang, J. Sui, H. E. Wang, W. Cai, G. Z. Cao, *Chem. Eng. J.* **2018**, *354*, 1164–1173.
[53] X. Zhao, H. E. Wang, Y. Yang, Z. G. Neale, R. C. Massé, J. Cao, W. Cai, J. H. Sui, G. Z. Cao, *Energy Storage Mater.* **2018**, *12*, 241–251.
[54] Y. Subramanian, G. K. Veerasubramani, M.-S. Park, D.-W. Kim, *J. Electrochem. Soc.* **2019**, *166*, A598–A604.
[55] S. K. Min, E. Lim, S. Kim, C. Jo, J. Chun, J. Lee, *Adv. Funct. Mater.* **2017**, *27*, 1603921.
[56] J. Zhao, G. L. Wang, R. Hu, K. Zhu, K. Cheng, K. Ye, D. X. Cao, Z. J. Fan, *J. Mater. Chem. A* **2019**, *7*, 4047–4054
[57] H. Zhang, R. J. Bai, C. Lu, J. Li, Y. G. Xu, L. B. Kong, M. C. Liu, *Ionics* **2018**, *25*, 533–540.
[58] S. Y. Dong, L. F. Shen, H. S. Li, P. Nie, Y. Y. Zhu, Q. Sheng, X. G. Zhang, *J. Mater. Chem. A* **2015**, *3*, 21277–21283.
[59] H. S. Li, L. L. Peng, Y. Zhu, X. G. Zhang, G. H. Yu, *Nano Lett.* **2016**, *16*, 5938–5943.
[60] S. S. M. Bhat, B. Babu, M. Feygenson, J. C. Neuefeind, M. M. Shaijumon, *ACS Appl. Mater. Interfaces* **2018**, *10*, 437–447.
[61] B. Babu, M. M. Shaijumon, *J. Power Sources* **2017**, *353*, 85–94.
[62] T. Y. Wei, G. Z. Yang, C. X. Wang, *ACS Appl. Mater. Interfaces* **2017**, *9*, 31861–31870.
[63] H.-K. Roh, M.-S. Kim, K. Y. Chung, M. Ulaganathan, V. Aravindan, S. Madhavi, K. C. Roh, K.-B. Kim, *J. Mater. Chem. A* **2017**, *5*, 17506–17516.
[64] R. Thangavel, B. Moorthy, D. K. Kim, Y.-S. Lee, *Adv. Energy Mater.* **2017**, *7*, 1602654.
[65] P. Tuan Ngoc, M. K. Gong, R. Thangavel, Y. S. Lee, C. H. Ko, *J. Alloys Compd.* **2018**, *743*, 639–645.
[66] R. Thangavel, K. Kaliyappan, K. Kang, X. Sun, Y. S. Lee, *Adv. Energy Mater.* **2016**, *6*, 1502199.
[67] L. Y. Wu, S. Y. Dong, G. Pang, H. S. Li, C. Y. Xu, Y. D. Zhang, H. Dou, X. G. Zhang, *J. Mater. Chem. A* **2019**, *7*, 1030–1037.
[68] R. Ding, L. Qi, H. Y. Wang, *Electrochim. Acta* **2013**, *114*, 726–735.
[69] T. Y. Wei, C. H. Chen, H. C. Chien, S. Y. Lu, C. C. Hu, *Adv. Mater.* **2010**, *22*, 347–351.
[70] Z. C. Yan, L. Liu, H. B. Shu, X. K. Yang, H. Wang, J. L. Tan, Q. Zhou, Z. F. Huang, X. Y. Wang, *J. Power Sources* **2015**, *274*, 8–14.
[71] D. A. Stevens, J. R. Dahn, *J. Electrochem. Soc.* **2000**, *147*, 1271–1273.
[72] a) X. W. Dou, I. Hasa, D. Saurel, C. Vaalma, L. M. Wu, D. Buchholz, D. Bresser, S. Komaba, S. Passerini, *Mater. Today* **2019**, *23*, 87–104; b) L. F. Xiao, Y. L. Cao, W. A. Henderson, M. L. Sushko, Y. Shao, J. Xiao, W. Wang, M. H. Engelhard, Z. M. Nie, J. Liu, *Nano Energy* **2016**, *19*, 279–288; c) B. W. Xiao, T. Rojo, X. L. Li, *ChemSusChem* **2019**, *12*, 133–144.
[73] J. Ajuria, E. Redondo, M. Arnaiz, R. Mysyk, T. Rojo, E. Goikolea, *J. Power Sources* **2017**, *359*, 17–26.
[74] K. Kuratani, M. Yao, H. Senoh, N. Takeichi, T. Sakai, T. Kiyobayashi, *Electrochim. Acta* **2012**, *76*, 320–325.
[75] Z. L. Jian, Z. Y. Xing, C. Bommier, Z. F. Li, X. L. Ji, *Adv. Energy Mater.* **2016**, *6*, 1501874.
[76] a) Y. Guo, Z. Q. Shi, M. M. Chen, C. Y. Wang, *J. Power Sources* **2014**, *252*, 235–243; b) Z. L. Jian, C. Bommier, L. L. Luo, Z. F. Li, X. L. Ji, *Chem. Mater.* **2017**, *29*, 2314–2320.
[77] P. X. Han, X. Q. Han, J. H. Yao, L. X. Zhang, X. Y. Cao, C. S. Huang, G. L. Cui, *J. Power Sources* **2015**, *297*, 457–463.
[78] Z. Ling, C. E. Ren, M. Q. Zhao, J. Yang, J. M. Giammarco, J. S. Qiu, M. W. Barsoum, Y. Gogotsi, *Proc. Mont. Acad. Sci.* **2014**, *111*, 16676–16681.
[79] N. Kurra, M. Alhabeb, K. Maleski, C.-H. Wang, H. N. Alshareef, Y. Gogotsi, *ACS Energy Lett.* **2018**, *3*, 2094–2100.
[80] J. M. Luo, J. H. Zheng, J. W. Nai, C. B. Jin, H. D. Yuan, O. W. Sheng, Y. J. Liu, R. Y. Fang, W. K. Zhang, H. Huang, Y. P. Gan, Y. Xia, C. Liang, J. Zhang, W. Y. Li, X. Y. Tao, *Adv. Funct. Mater.* **2019**, *29*, 1808107.
[81] X. Wang, S. Kajiyama, H. Iinuma, E. Hosono, S. Oro, I. Moriguchi, M. Okubo, A. Yamada, *Nat. Commun.* **2015**, *6*, 6544.
[82] X. Q. Xie, M. Q. Zhao, B. Anasori, K. Maleski, C. E. Ren, J. W. Li, B. W. Byles, E. Pomerantseva, G. X. Wang, Y. Gogotsi, *Nano Energy* **2016**, *26*, 513–523.
[83] J. M. Luo, C. Fang, C. B. Jin, H. D. Yuan, O. W. Sheng, R. Y. Fang, W. K. Zhang, H. Huang, Y. P. Gan, Y. Xia, C. Liang, J. Zhang, W. Y. Li, X. Y. Tao, *J. Mater. Chem. A* **2018**, *6*, 7794–7806.
[84] D. M. Xu, D. L. Chao, H. W. Wang, Y. S. Gong, R. Wang, B. B. He, X. L. Hu, H. J. Fan, *Adv. Energy Mater.* **2018**, *8*, 1702769.
[85] Q. L. Wei, Y. L. Jiang, X. S. Qian, L. Zhang, Q. D. Li, S. S. Tan, K. N. Zhao, W. Yang, Q. Y. An, J. H. Guo, L. Q. Mai, *iScience* **2018**, *6*, 212–221.
[86] K. Kaliyappan, Z. W. Chen, *Nano Energy* **2018**, *48*, 107–116.
[87] S. Qiu, L. F. Xiao, M. L. Sushko, K. S. Han, Y. Y. Shao, M. Y. Yan, X. M. Liang, L. Q. Mai, J. W. Feng, Y. L. Cao, X. P. Ai, H. X. Yang, J. Liu, *Adv. Energy Mater.* **2017**, *7*, 1700403.
[88] K. Krishnamoorthy, P. Pazhamalai, S. Sahoo, J. H. Lim, K. H. Choi, S. J. Kim, *ChemElectroChem* **2017**, *4*, 3302–3308.
[89] K. Lu, B. Song, X. Gao, H. X. Dai, J. T. Zhang, H. Y. Ma, *J. Power Sources* **2016**, *303*, 347–353.

[90] S. Gao, J. C. Zhao, Y. Zhao, Y. D. Wu, X. Zhang, L. L. Wang, X. J. Liu, Y. C. Rui, J. L. Xu, *Mater. Lett.* **2015**, *158*, 300–303.
[91] S. Y. Wang, J. C. Zhao, L. L. Wang, X. J. Liu, Y. D. Wu, J. L. Xu, *Ionics* **2015**, *21*, 2633–2638.
[92] L. Zhou, Z. K. Yang, C. Y. Li, B. W. Chen, Y. F. Wang, L. J. Fu, Y. S. Zhu, X. Liu, Y. P. Wu, *RSC Adv.* **2016**, *6*, 109340–109345.
[93] H. C. Gu, L. J. Kong, H. J. Cui, X. L. Zhou, Z. J. Xie, Z. Zhou, *J. Energy Chem.* **2019**, *28*, 79–84.
[94] a) S. J. Wang, R. T. Wang, Y. B. Zhang, D. D. Jin, L. Zhang, *J. Power Sources* **2018**, *379*, 33–40; b) J. Ding, Z. Li, K. Cui, S. Boyer, D. Karpuzov, D. Mitlin, *Nano Energy* **2016**, *23*, 129–137.
[95] a) H. L. Wang, D. Mitlin, J. Ding, Z. Li, K. Cui, *J. Mater. Chem. A* **2016**, *4*, 5149–5158; b) X. Liu, H. L. Wang, Y. P. Cui, X. N. Xu, H. Zhang, G. F. Lu, J. Shi, W. Liu, S. G. Chen, X. Wang, *J. Mater. Sci.* **2018**, *53*, 6763–6773.
[96] J. Ding, H. L. Wang, Z. Li, K. Cui, D. Karpuzov, X. H. Tan, A. Kohandehghan, D. Mitlin, *Energy Environ. Sci.* **2015**, *8*, 941–955.
[97] B. J. Yang, J. T. Chen, S. L. Lei, R. S. Guo, H. X. Li, S. Q. Shi, X. B. Yan, *Adv. Energy Mater.* **2018**, *8*, 1702409.
[98] S. Y. Dong, Y. L. Xu, L. Y. Wu, H. Dou, X. G. Zhang, *Energy Storage Mater.* **2018**, *11*, 8–15.
[99] S. Y. Cho, H. J. Yoon, N. R. Kim, Y. S. Yun, H.-J. Jin, *J. Power Sources* **2016**, *329*, 536–545.
[100] Y. Y. Ding, B. J. Yang, J. T. Chen, L. Zhang, J. S. Li, Y. L. Li, X. B. Yan, *Science China-Materials* **2018**, *61*, 285–295.
[101] S. H. Chen, J. Wang, L. Fan, R. F. Ma, E. J. Zhang, Q. Liu, B. A Lu, *Adv. Energy Mater.* **2018**, *8*, 1800140.
[102] C. Wang, F. X. Wang, Z. C. Liu, Y. J. Zhao, Y. Liu, Q. Yue, H. W. Zhu, Y. H. Deng, Y. P. Wu, D. Y. Zhao, *Nano Energy* **2017**, *41*, 674–680.
[103] L. Yin, J. L. Feng, X. H. Zhang, L. Li, J. S. Liu, H. He, Y. X. Lin, *J. Mater. Sci.* **2018**, *54*, 4124–4134.
[104] M. Y. Liu, J. Niu, Z. P. Zhang, M. L. Dou, Z. L. Li, F. Wang, *J. Power Sources* **2019**, *414*, 68–75.

Manuscript received: June 9, 2019
Revised manuscript received: July 18, 2019
Accepted manuscript online: July 21, 2019
Version of record online: August 7, 2019